

Explosion sites of SN 1994W-like transients

E. Kankare^{1,2,*}, T. Kangas^{3,1}, M. Fraser⁴, S. Mattila^{1,5}, A. Pastorello⁶, N. Elias-Rosa^{6,7}, G. Altavilla^{8,9},
S. Benetti⁶, R. Kotak¹, K. Matilainen¹, and I. Mäntynen¹

- ¹ Department of Physics and Astronomy, University of Turku, 20014 Turku, Finland
- ² Turku Collegium for Science, Medicine and Technology, University of Turku, 20014 Turku, Finland
- ³ Finnish Centre for Astronomy with ESO (FINCA), 20014 University of Turku, Finland
- ⁴ School of Physics, O'Brien Centre for Science North, University College Dublin, Belfield, Dublin 4, Ireland
- ⁵ School of Sciences, European University Cyprus, Diogenes street, Engomi, 1516 Nicosia, Cyprus
- ⁶ INAF – Osservatorio Astronomico di Padova, vicolo dell'Osservatorio 5, 35122 Padova, Italy
- ⁷ Institute of Space Sciences (ICE, CSIC), Campus UAB, Carrer de Can Magrans s/n, 08193 Barcelona, Spain
- ⁸ INAF – Osservatorio Astronomico di Roma, Via Frascati, 33, 00078 Monte Porzio Catone (RM), Italy
- ⁹ SSDC-ASI, Via del Politecnico, snc, 00133 Roma, Italy

Received 27 March 2025 / Accepted 22 May 2025

ABSTRACT

We study a sample of narrow-line transients that share characteristics with the Type II_n classified supernova (SN) 1994W, a prototypical member of this class of events, via an investigation of their explosion sites and spectrophotometric data. The normalised cumulative rank (NCR) method was used to compare the explosion sites of ten events to the star formation distributions of their host galaxies, and to the sites of different evolved massive stars. The resulting sample mean value of $NCR_{H\alpha} = 0.170 \pm 0.076$ is low, while the NCR_{NUV} distribution is flat with a mean value of 0.488 ± 0.084 . The NCR distribution of SN 1994W-like events is consistent with relatively low-mass red supergiants (RSGs) and, despite the small sample size, inconsistent with high-mass stars such as luminous blue variables. To explain the nature of SN 1994W-like transients, an interaction between an expanding ejecta and a relatively massive circumstellar medium is likely required, with the latter possibly having been produced by a H envelope ejection via a nuclear flash event, or a luminous red nova (LRN) from a stellar merger; both channels are consistent with the low-mass RSGs suggested by the NCR results. In this context, we find the early -26 d spectrum from light curve maximum of SN 2003G to have similarities to those of F8-type supergiant stars and LRNe. Finally, based on late-time HST imaging, we set the deepest limits for the surviving precursor of SN 2011ht to $M_{F438W} > -3.8$ and $M_{F555W} > -4.0$ mag. This would exclude most supergiants as a non-terminal progenitor, assuming that such a star is not completely obscured by newly formed dust.

Key words. supernovae: general

1. Introduction

In the commonly adopted classification scheme of supernova (SN) explosions (Filippenko 1997), Type II_n SNe are a category of stellar transients characterised by SN-like luminosities, hydrogen lines (thus Type II, contrary to H-poor Type I SNe), and narrow (thus Type II_n) line profiles with a full width at half maximum (FWHM) of $\lesssim 10^3$ km s⁻¹. However, in some cases contamination through host galaxy lines or early narrow spectral features of normal Type II SNe can result in misclassification. The narrow lines of Type II_n SNe are thought to arise from the ionised unshocked circumstellar medium (CSM) and the events to be powered by a shock interaction of the SN ejecta with the CSM. By definition, core-collapse SNe (CCSNe) are terminal explosions that end the life cycles of massive stars. However, the SN nature of the Type II_n classified SN 1994W and similar events has been debated (e.g. Dessart et al. 2009).

In this work, we study a sample of spectroscopically SN 1994W-like transients; these events have very similar properties overall. Photometrically, most of these transients show a Type IIP SN-like flat ~ 100 d light curve plateau followed by a sharp drop in luminosity, and a subsequent tail phase with decline rates that can notably vary (e.g. Sollerman et al.

1998; Kankare et al. 2012). Occasionally the SN 1994W-like events are also dubbed as Type II_n-P SNe (e.g. Mauerhan et al. 2013), where the ‘P’ indicates the presence of a plateau. During the plateau phase, the spectra are dominated by prominent H lines, accompanied by a large number of metal lines that appear roughly at $+30$ d, including for example Fe II, Ti II, and Ca II (e.g. Dessart et al. 2009). These spectral features have distinct narrow P Cygni profiles with broad emission wings. The absorption minima of these P Cygni profiles have blueshifted velocities (hereafter P Cygni velocities) that in the case of H α profiles of SN 1994W-like events appear to typically have a very narrow range of ~ 600 to 700 km s⁻¹ during the initial ~ 100 d (e.g. Chugai et al. 2004; Kankare et al. 2012). If the observations have been obtained with a poor spectral resolution, these velocities can appear artificially larger, or the absorption components are not detected at all. The broad line profile wings of SN 1994W-like events likely arise from multiple electron scattering (Dessart et al. 2009); therefore, these are not kinematically distinct high-velocity components. Furthermore, the early spectra of these transients display low H α /H β ratios, which can approach $L_{H\alpha}/L_{H\beta} \approx 1$ (e.g. Kankare et al. 2012). Collisional de-excitation effects can reduce the H α /H β ratio below the typical case B recombination coefficient at high electron densities (Drake & Ulrich 1980). However, at late times, in the tail phase,

* Corresponding author: erkki.kankare@utu.fi

the spectra show large $H\alpha/H\beta$ ratios, similar to many other Type II_n SNe. In the light curve tail epochs, normal Type IIP SNe have entered into the nebular phase with optically thin ejecta and show broad emission lines that typically include prominent forbidden lines such as [O I] $\lambda\lambda 6300, 6364$. In the post-plateau spectra, the electron scattering wings of SN 1994W-like events have disappeared, but broad nebular emission lines remain absent (e.g. Chugai et al. 2004; Kankare et al. 2012). A compilation of radio observations of CCSNe by Bietenholz et al. (2021) cover a few SN 1994W-like events; however, those only resulted in upper limits for these transients.

Various origin channels have been discussed to explain the nature of SN 1994W-like events, including fallback SNe (Sollerman et al. 1998; Mauerhan et al. 2013; Elias-Rosa et al. 2024), electron-capture SNe (Kankare et al. 2012; Mauerhan et al. 2013; Moriya et al. 2014), SN impostors via collisions of non-terminal stellar outburst shells (Dessart et al. 2009) or specific outflow configurations (Humphreys et al. 2012), SNe with a high CSM mass of $M_{\text{CSM}} \geq M_{\text{ejecta}}$ (Dessart et al. 2010, 2016; Kankare et al. 2012), or SNe with other specific ejecta and CSM properties (Sollerman et al. 1998; Chugai et al. 2004; Roming et al. 2012; Li & Morozova 2022; Elias-Rosa et al. 2024).

Characteristics of SN 1994W-like events suggest that a high CSM mass compared to the ejecta mass would be required to explain these events. A strong mass-loss episode could happen via envelope ejection for which nuclear flashes or binary system mergers are potential channels. The binding energies are low, $\sim 10^{47}$ erg, for the extended H envelopes of red supergiants (RSGs) with main-sequence masses up to $\sim 25 M_{\odot}$ (Dessart et al. 2010). It has been suggested that neon or silicon flashes of $\sim 10 M_{\odot}$ stars could lead to the ejection of the H envelope on timescales of a few years or less before a CCSN explosion (Woosley et al. 2002; Woosley & Heger 2015). Based on numerical simulations of 10–25 M_{\odot} stars, Dessart et al. (2010) suggested that a shell-burning-associated nuclear flash of such stars could result in an envelope ejection event that resembles a faint Type IIP SN or a SN impostor with a distinct light curve plateau, which could explain events such as SN 1994W, by way of a massive eruption of CSM in the few years running up to the SN explosion.

Luminous red novae (LRNe) are transients that show double-peaked light curves that reach magnitudes of -13 to -15 mag. Typically, the first peak evolves rapidly and is blue in colour, whereas the second peak is red, slower, and in some cases plateau-like. The spectra of the events show narrow P Cygni Balmer lines, Fe II features, and other metal lines. Several case studies of such events have been carried out (Smith et al. 2016; Blagorodnova et al. 2017, 2021; Lipunov et al. 2017; MacLeod et al. 2017; Cai et al. 2019, 2022; Pastorello et al. 2019a,b, 2021a,b, 2023; Stritzinger et al. 2020). Ivanova et al. (2013) and Metzger & Pejcha (2017) have discussed the contextual similarity of LRNe and fainter red novae, suggesting that LRNe arise from contact binary systems that experience a common envelope event. The pre-outburst mass loss would occur primarily in an equatorial direction powered by the conservation of angular momentum of the secondary star engulfed in the envelope, decreasing the orbital separation and resulting in a slow light curve rise (e.g. ~ 200 d in the case of the Galactic red nova V1309 Sco; Tylenda et al. 2011), which can be followed by a complete common envelope ejection or a merger with partial mass ejection, resulting in a double-peaked transient. Metzger & Pejcha (2017) suggest a model in which the first blue peak of red novae arise from thermal radi-

ation of a hot and cooling symmetrical outburst ejecta seen unobscured in the polar direction. MacLeod et al. (2017) and Matsumoto & Metzger (2022) have suggested that H recombination powers the red peak, though it has also been suggested that an interaction with potentially equatorial low-velocity CSM can dominate or contribute to the powering of this phase (e.g. Metzger & Pejcha 2017; Matsumoto & Metzger 2022). The common envelope events could also be a mechanism to produce a CSM mass sufficiently large to explain the SN 1994W-like events (e.g. Ercolino et al. 2024).

Section 2 describes the pixel statistics analysis carried out on the correlation of a sample of SN 1994W-like transients and the host galaxy $H\alpha$ and ultraviolet (UV) emission. Section 3 covers the new follow-up data of SN 1999eb. Section 4 explores the archival data of SN 2003G, which include an early -26 d spectrum of the event. We note that the redshift time-dilation effects for our nearby sample of events are typically quite small ($\lesssim 1$ d) for the considered epochs, which are provided in the observer frame unless otherwise noted. Section 5 contains an inspection of late-time *Hubble* Space Telescope (HST) archival images of the explosion site of SN 1994W-like events. Sections 6 and 7 provide the discussion and the conclusions, respectively.

2. Statistical analysis of SN 1994W-like events

2.1. Sample of SN 1994W-like events

This section lists the SN 1994W-like events adopted in our analysis, which likely share a similar physical origin. A spectroscopic time series is shown in Fig. 1 with a selection of spectra of some of these transients to stress their homogenous evolution. Similarly, a light curve comparison is shown in Fig. 2. The basic parameters of the sample transients are presented in Table 1. Preceding our observations for the statistical study, the sample was selected based on classified Type II_n SNe that were stated in telegrams or journal publications to spectroscopically resemble SN 1994W or other events previously identified as SN 1994W-like. Further details on these reports are provided in the following subsections for each target. Unfortunately, classification descriptions do not necessarily explicitly state similarities to SN 1994W-like events or the observations are not obtained with sufficiently high resolution and signal-to-noise ratio to identify SN 1994W-like characteristics. Therefore, our sample is likely missing potential events; however, those should not be particularly biased towards any specific environments.

2.1.1. SN 1994W

SN 1994W was discovered by Cortini et al. (1994) in NGC 4041 on Julian date (JD) 2449563.35. The event was classified as a Type II SN with narrow Balmer lines based on observations on JD 2449565.4 by Bragaglia et al. (1994) and on JD 2449568.5 by Filippenko & Barth (1994), with the latter reporting P Cygni velocities of 700 km s^{-1} . In their spectrophotometric study, Sollerman et al. (1998) estimated a ^{56}Ni mass of $\lesssim 0.0026 M_{\odot}$ and suggested that the event was either a low-energy explosion of a massive star with a low zero age main sequence (ZAMS) mass ($M_{\text{ZAMS}} \approx 8$ to $10 M_{\odot}$), or a fallback SN from a high-mass ($M_{\text{ZAMS}} \geq 25 M_{\odot}$) progenitor, with the latter scenario favoured. Chugai et al. (2004) carried out modelling of the light curves and $H\alpha$ line profile evolution of SN 1994W, and suggested that the event was a Type II_n SN with an ejecta mass of around $8 M_{\odot}$ embedded in a $0.4 M_{\odot}$ envelope of CSM. However, Dessart et al. (2016) pointed out based on further

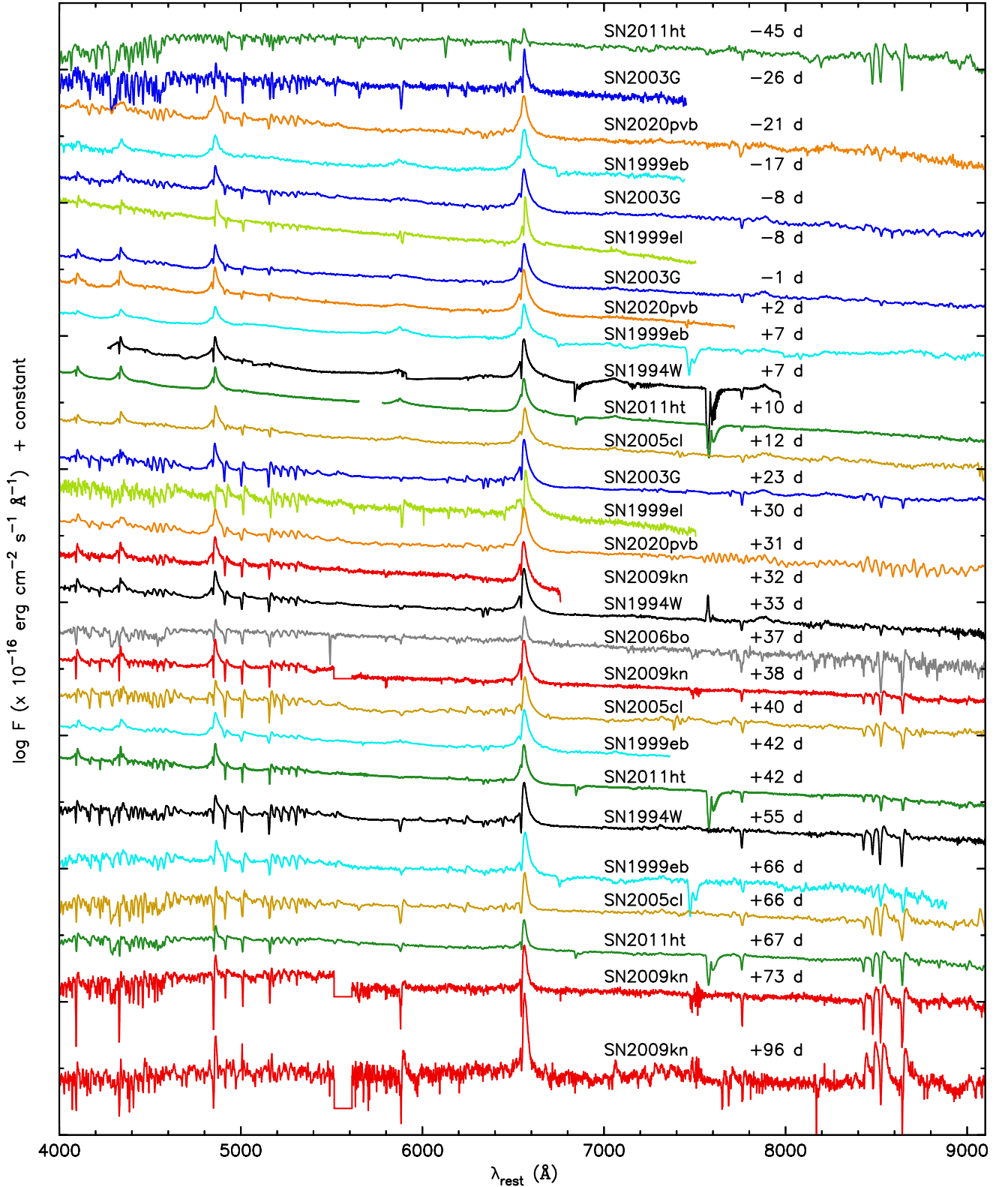


Fig. 1. Selection of spectra of a sample SN 1994W-like events, including SNe 1994W (Chugai et al. 2004), 1999eb (see Sect. 3), 1999el (see Sect. 2.1.4), 2003G (Shivvers et al. 2017), 2005cl (Kiewe et al. 2012), 2006bo (Taddia et al. 2013), 2009kn (Kankare et al. 2012), 2011ht (Humphreys et al. 2012; Pastorello et al. 2019b), and 2020pvb (Elias-Rosa et al. 2024). The spectra were dereddened by the total line-of-sight extinction estimates and the wavelengths corrected to the host galaxy rest frame.

hydrodynamical and radiative transfer simulations that such a scenario would struggle not to produce broad lines at late times, which were absent in SN 1994W, and would instead result in a SN 1998S-like event (Fassia et al. 2001). Dessart et al.

(2009) carried out radiative transfer modelling of SN 1994W and found that the plateau phase line profiles, with broad wings included, can be produced by electron scattering via a single region of radiation in a slowly expanding material; based on

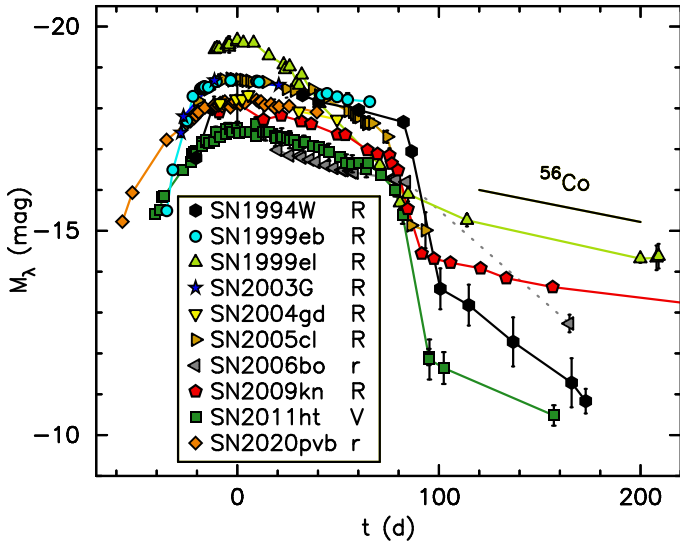


Fig. 2. Absolute light curve selection of spectroscopically SN 1994W-like events. The epoch $t = 0$ d corresponds to the estimated light curve peak. The sample includes SNe 1994W (Sollerman et al. 1998, and references therein), 1999eb (see Sect. 3), 1999el (Di Carlo et al. 2002), 2003G (see Sect. 4), 2004gd (see Sect. 4), 2005cl (Kiewe et al. 2012), 2006bo (Taddia et al. 2013), 2009kn (Kankare et al. 2012), 2011ht (Roming et al. 2012; Humphreys et al. 2012; Mauerhan et al. 2013), and 2020pvb (Elias-Rosa et al. 2024). The R -band light curve of SN 1994W was partly generated based on the B and V -band observations of the event, and the colour evolution of SN 2009kn. The luminosity slope is shown for the radioactive decay of ^{56}Co assuming complete γ -ray trapping.

the absence of broad emission line components and low ^{56}Ni mass estimates they also speculated with the possibility that the event could have been powered by a collision of ejected shells from non-terminal stellar explosions. Based on their simulations, Dessart et al. (2016) favoured a model of fast-moving but less massive SN ejecta interacting with a more massive CSM shell ($M_{\text{CSM}} > M_{\text{ejecta}}$) to explain the observational characteristics of SN 1994W.

2.1.2. SN 1994ak

Nakano et al. (1994) reported the discovery of SN 1994ak in NGC 2782 with the earliest detection on JD 2449711.36. A Type II_n classification spectrum of SN 1994ak was obtained by Garnavich et al. (1995) on JD 2449714.95 and reported that it showed strong Balmer lines with a narrow emission component on a broad base, and P Cygni velocities of 600 km s^{-1} . No detailed analysis of SN 1994ak has been published; however, Filippenko (1997, see their Figure 14) presented in the review of CCSN subtypes an optical spectrum of SN 1994ak obtained on JD 2449744, which shows narrow P Cygni Balmer and Fe II lines similar to SN 1994W-like events.

2.1.3. SN 1999eb

Modjaz et al. (1999) reported the discovery of SN 1999eb in NGC 664 using the 0.8 m Katzman Automatic Imaging Telescope (KAIT) with the earliest unfiltered 19.0 mag detection on JD 2451440.5 and three additional epochs of early photometry that showed a light curve rise. We adopted these observations as approximate R -band magnitudes. Garnavich et al. (1999) obtained a spectrum of the event on JD 2451454.8, and reported

Balmer lines with P Cygni velocities of 900 km s^{-1} , P Cygni Fe II lines, and an overall similarity to that of SN 1995G¹. Li et al. (2002) presented HST late-time F555W and F814W band observations of SN 1999eb, which we adopted as approximate V and I -band magnitudes, respectively (Sect. 3).

2.1.4. SN 1999el

SN 1999el was discovered in NGC 6951 on JD 2451471.95. Cao et al. (1999) reported the discovery and classification of the event as a Type II_n SN. Di Carlo et al. (2002) carried out a spectrophotometric follow-up study of the transient and concluded that the event was a Type II_n SN with a rapidly declining light curve, which showed narrow Balmer lines with broad wings and P Cygni velocities of $600\text{--}900 \text{ km s}^{-1}$; the spectroscopic similarity to that of SN 1999eb was pointed out in the study. They suggested that SN 1999el had a progenitor with a history of asymmetric mass-loss episodes and a near-infrared (near-IR) excess that arose likely from pre-existing circumstellar dust. Similar to SN 1999eb, Li et al. (2002) reported HST late-time F555W and F814W band observations of SN 1999el. Spectroscopically, SN 1999el is very similar to SN 1994W-like transients, and has a linear Type III SN-like light curve evolution; therefore, a distinctive Type IIP SN-like plateau and a subsequent light curve drop are not necessarily characteristics that define this type of event.

One spectrum of SN 1999el was reported by Shivvers et al. (2017) in their compilation of SN data, and the Weizmann Interactive Supernova Data Repository (WiSeREP; Yaron & Gal-Yam 2012) hosts six additional epochs of spectra with no available information on the used instruments. The host galaxy extinction of SN 1999el is uncertain; therefore, we carried out a comparison between the spectrum in WiSeREP of SN 1999el observed +30 d after the light curve peak and dereddened with a range of different host galaxy extinctions, and the spectrum of SN 2009kn which was deemed to have been obtained roughly +32 d after the light curve peak. This suggests a host galaxy extinction of $A_{V,\text{host}} \approx 1.5 \text{ mag}$ to result in similar colours (Fig. 1). Combined with the Galactic extinction of $A_{V,\text{Gal}} = 1.020 \text{ mag}$ this is consistent with the high-end estimate of Di Carlo et al. (2002) with an accompanying ^{56}Ni mass estimate of $\leq 0.07 M_{\odot}$.

2.1.5. SN 2003G

Graham et al. (2003) reported the discovery of SN 2003G in IC 208 on JD 2452647.7 with an unfiltered magnitude of 16.2 mag, and an additional imaging on JD 2452649.0 with 15.8 mag, which we adopt directly as R -band magnitudes. The classification spectrum was obtained by Hamuy & Maza (2003) on JD 2452648.55, which they note to show strong similarity to SN 1994W with line profiles that have narrow emission and absorption components and broad bases. No detailed study of the event has been reported; however, four spectra are available in WiSeREP, which we adopted to our analysis (Sect. 4).

¹ SN 1995G showed spectroscopic similarity to SN 1994W-like events with P Cygni profile in Balmer and Fe II lines that have blueshifted absorption minimum velocities of $\sim 700 \text{ km s}^{-1}$; however, the event has also a very slow light curve evolution of $\sim 5 \text{ mag}$ in 2.5 yr (Pastorello et al. 2002). It is unclear if SN 1995G shares the origin channel with other SN 1994W-like transients discussed here, and conservatively it was not included in our sample. Similarly, while the early spectra of SN 2011A (de Jaeger et al. 2015) resemble SN 1994W-like events, the later spectral evolution differ and the event was not included in the sample.

Table 1. Adopted parameters of the analysed sample of SN 1994W-like events.

SN	α^a	δ^a	Host	z^b	D_L^c (Mpc)	μ (mag)	$A_{V, Gal}^d$ (mag)	$A_{V, host}^e$ (mag)	$t_{peak, JD}$
1994W	12:02:11.01	+62:08:31.8	NGC 4041	0.004116	24.4	31.94	0.049	–	2449571.5
1994ak	09:14:01.47	+40:06:21.5	NGC 2782	0.008483	41.5	33.09	0.044	–	–
1999eb	01:43:45.45	+04:13:25.9	NGC 664	0.018096	76.8	34.43	0.074	0.0	2451475.9
1999el	20:37:17.72	+66:06:11.5	NGC 6951	0.004750	25.5	32.03	1.020	1.5	2451490.6
2003G	02:08:28.13	+06:23:51.9	IC 208	0.011755	49.5	33.47	0.149	0.0	2452675.7
2004F	03:17:53.80	–07:17:43.0	NGC 1285	0.017475	74.1	34.35	0.150	–	–
2004gd	07:09:11.71	+20:36:10.6	NGC 2341	0.017215	76.4	34.42	0.198	1.0	2453324.5
2005cl	21:02:02.35	–06:17:35.7	MCG -01-53-020	0.025878	116.0	35.32	0.194	–	2453556.5
2006bo	20:30:41.90	+09:11:40.8	UGC 11578	0.015347	70.6	34.24	0.283	–	2453814.9
2009kn	08:09:43.04	–17:44:51.3	ESO 561- G 020	0.015798	71.8	34.28	0.306	0.0	2455140.0
2011ht	10:08:10.59	+51:50:57.0	UGC 5460	0.003646	21.4	31.65	0.029	0.19	2455879.5
2020pvb	20:53:53.03	–25:28:26.1	NGC 6993	0.020277	90.3	34.78	0.187	0.15	2459159.8

Notes. ^(a) SN coordinates from the Transient Name Server (TNS), except for SN 1994W (see Sect. 5.1). ^(b) Redshifts via the NASA/IPAC Extragalactic Database (see references therein). ^(c) Virgo + Great Attractor corrected luminosity distance (Mould et al. 2000) assuming $H_0 = 69.6 \text{ km s}^{-1} \text{ Mpc}^{-1}$ (Bennett et al. 2014). ^(d) Galactic line-of-sight extinction values from Schlafly & Finkbeiner (2011). ^(e) Host extinction estimates from the literature for SNe 2009kn (Kankare et al. 2012), 2011ht (Roming et al. 2012), 2020pvb (Elias-Rosa et al. 2024), or from this work for SNe 1999eb, 1999el, 2003G, and 2004gd. Otherwise, negligible host galaxy extinction was assumed.

2.1.6. SN 2004F

Swift et al. (2004) reported the discovery of SN 2004F in NGC 1285 on JD 2453020.7 with an unfiltered magnitude of 17.8 mag. The reported unfiltered VSNET magnitude² of 17.1 mag on JD 2453029.34 suggests that the light curve was rising and corresponds to an absolute magnitude of roughly -17.4 mag. Filippenko et al. (2004) reported classification spectra of SN 2004F obtained around JD 2453049, and noted that SN 2004F resembles SNe 1994W and 1994ak with narrow emission lines and P Cygni velocities of 800 km s^{-1} . They noted that Ca II, O I, Fe II, and Na I features were present in the spectrum.

2.1.7. SN 2004gd

Moore et al. (2004) reported the discovery of SN 2004gd in NGC 2341 on JD 2453315.95 with an unfiltered magnitude of 18.3 mag, and three additional follow-up epochs that cover a slow light curve rise. We adopted these observations as approximate *R*-band magnitudes. Filippenko & Foley (2004) obtained a spectrum of SN 2004gd on JD 2453352, and reported that it resembled SN 1995G with narrow emission lines on a broad base and P Cygni velocities of 700 km s^{-1} .

2.1.8. SN 2005cl

SN 2005cl was discovered in MCG -01-53-020 by Pugh & Li (2005) with the earliest detection on JD 2453523.97. Modjaz et al. (2005) reported a spectroscopic classification on JD 2453534.93 as a Type IIn SN with a blue continuum and Balmer emission lines with narrow and broad components. Spectrophotometric follow-up data of SN 2005cl was presented in a compilation of four Type IIn SNe by Kiewe et al. (2012), reporting narrow P Cygni profiles of Balmer lines and an overall spectrophotometric similarity to that of SN 1994W. Their optical photometry covered a plateau length of roughly 100 d, which turned to a more rapid decline. Li & Morozova (2022) used

² http://www.astrosurf.com/snweb2/2004/04F_/04F_Meas.htm

a radiation hydrodynamics simulation grid to model the light curve evolution of SN 2005cl, and suggested that SN 1994W-like events could be explained as $M_{ZAMS} \approx 10$ to $15 M_{\odot}$ RSG progenitors that have experienced a $\sim 10^{47}$ erg outburst several months before the final SN explosion (best fit 258 d before the onset of SN 2005cl suggested by their models).

2.1.9. SN 2006bo

Boles & Monard (2006) reported the discovery of SN 2006bo in UGC 11578 with the earliest detection on JD 2453830.65. Blondin et al. (2006) classified the event as a Type IIn SN based on a spectrum obtained on JD 2453851.01. The compilation of five Type IIn SNe by Taddia et al. (2013) included a follow-up study of SN 2006bo, which they identified as a SN 1994W-like event with Balmer and Fe II lines that show narrow emission components and P Cygni velocities of 600 km s^{-1} . The photometry of SN 2006bo does not cover the rise and the explosion date is uncertain as the pre-discovery non-detection on JD 2453703 does not provide a strong constraint. The photometric observations of SN 2006bo by Taddia et al. (2013) started on JD 2453834.92. Based on the light curve evolution and the continuum shape of the SN 2006bo spectrum obtained on JD 2453841.5, we estimated that their photometric follow-up observations started roughly 20 d after the light curve maximum.

2.1.10. SN 2009kn

Gagliano et al. (2009) discovered SN 2009kn in ESO 561- G 020 on JD 2455130.96. Steele et al. (2009) reported the classification of SN 2009kn as a Type IIn SN based on a spectrum obtained on JD 2455145 and noted strong Balmer emission lines and narrow absorption components. Kankare et al. (2012) carried out a detailed follow-up study of the event, showed that it had twin-like characteristics compared to those of SN 1994W, and discussed the origin scenario of a SN with a massive CSM (including a variation of an electron-capture SN with an ambient medium of an ejected stellar envelope); the late-time photometry was found to be roughly consistent with a radioactive decay tail with a ^{56}Ni mass estimate of $0.023 M_{\odot}$. Based

on light curve modelling, [Moriya et al. \(2014\)](#) suggested that an electron-capture SN from a super-AGB star could produce a -17 mag transient with a H recombination powered plateau somewhat similar to SN 2009kn.

2.1.11. SN 2011ht

[Boles et al. \(2011\)](#) discovered SN 2011ht in UGC 5460 on JD 2455833.68. [Pastorello et al. \(2011\)](#) reported a spectroscopic classification of the event on JD 2455834.72 and considered the event to be a SN impostor, noted narrow P Cygni spectral line profiles, and listed detections of H I, Ca II, Fe II, Na I D, Sc II, and Ba II. Early *Swift* observations of the event were reported by [Roming et al. \(2011\)](#). [Prieto et al. \(2011\)](#) classified the event as a Type IIn SN based on a spectrum obtained on JD 2455877.0, and reported Balmer lines with narrow and broad emission components, and P Cygni velocities of 700 km s^{-1} . [Roming et al. \(2012\)](#) noted that SN 2011ht showed dense stellar wind-like spectral characteristics that resembled some SN impostors, but had the energy of a terminal SN explosion. They discussed the possibility of a dense shell of CSM ejected ~ 1 yr before the SN and shocked by the subsequent explosive transient. [Humphreys et al. \(2012\)](#) noted that observationally SN 2011ht was remarkably similar to that of SN 1994W, the inferred radiated energy of SN 2011ht was relatively low, and a likely origin for the event would be a continuous outflow with an onset ~ 0.5 yr before the discovery followed by outflow acceleration or a high-velocity mass-loss episode. However, [Mauerhan et al. \(2013\)](#) argued that a wind-like outflow would require an unphysically high Eddington factor of ~ 1000 to explain the event. They also found the tail phase of SN 2011ht to be consistent with radioactive decay of ^{56}Co when the near-IR excess associated with dust formation was included in the pseudo-bolometric light curve, resulting in a low estimated ^{56}Ni mass range of 0.006 to $0.01 M_{\odot}$, and suggested the event to be a terminal SN explosion, possibly either from an electron-capture SN or from a fallback SN, interacting with a dense CSM.

[Fraser et al. \(2013\)](#) and [Ofek et al. \(2014\)](#) reported precursor outburst detections of SN 2011ht, which resulted in a combined coverage within epochs -367 to -185 d before the maximum of SN 2011ht adopted here. [Pastorello et al. \(2019b\)](#) referred to this pre-outburst transient as UGC 5460-2010OT1 and discussed the similarity of the early spectrum of SN 2011ht, at -45 d before our adopted light curve peak, with that of a LRN NGC 4490-2011OT1 during the red peak. Furthermore, the light curve of NGC 5460-2010OT1 shares contextual similarity to those of double-peaked LRNe. Based on these characteristics, it was suggested that the precursor of SN 2011ht could have been a merger that had powered a LRN event.

2.1.12. SN 2020pvb

The discovery of SN 2020pvb in NGC 6993 was reported by [Chambers et al. \(2020\)](#). As discussed by [Elias-Rosa et al. \(2024\)](#), the early pre-outburst detection of $m_w = 21.04$ mag on JD 2459048.92 was followed by non-detections and a subsequent brightening to the main SN-like event with the first detection on JD 2459099.87. The transient was classified as a Type IIn SN on JD 2459138.3 by [Perley et al. \(2020\)](#). [Elias-Rosa et al. \(2024\)](#) report the detailed study of SN 2020pvb, which showed that it was a SN 1994W-like event and concluded that the transient could be a fallback SN from a massive progenitor, or a SN from a moderate or low-mass progenitor with a dense CSM.

2.2. NCR analysis of SN 1994W-like events

[Fruchter et al. \(2006\)](#) presented the statistical pixel analysis method in a correlation study of a sample of gamma-ray bursts and their host galaxy rest-frame UV/blue light. Subsequently, the normalised cumulative rank (NCR) method has been used to study CCSN subtypes via their correlations with host galaxy emission, in particular in H α (e.g. [James & Anderson 2006](#); [Anderson et al. 2012](#); [Kangas et al. 2013](#)). Furthermore, [Kangas et al. \(2017\)](#) compared the NCR results from CCSNe to those of massive stars in nearby galaxies. We carried out an NCR analysis of a sample of ten spectroscopically SN 1994W-like events (Sect. 2.1) to constrain their progenitor mass range. SNe 2005cl and 2020pvb were not included in the NCR sample due to their large distances of 116 and 90 Mpc, respectively, to avoid systematic uncertainties ([Kangas et al. 2017](#)).

2.2.1. NCR method

In the NCR method, the pixels of a galaxy image are ranked from faintest to brightest in an ascending order. The NCR value of each pixel is defined as a fraction of the host emission that originates in pixels with lower brightness. If the bias and sky background level, and in the case of line emission (e.g. H α) the galaxy continuum, have been accurately subtracted, the average pixel value p outside the galaxy is 0. Therefore, if the sum of the ascending pixel values is ≤ 0 , the NCR value is set to 0; this is the background. If the sum is > 0 , these are the regions of host galaxy emission, and the NCR value is defined as $\text{NCR}(n) = \sum_{i=1}^n p_i / p_{\text{tot}}$, where p_{tot} is the pixel value sum over the whole image and n is the n^{th} pixel in the ascending order. The exact image size does not affect the results. The NCR values of the pixels associated with sample target coordinates are a tracer of any correlation between the targets and the underlying host emission, and can be used for statistical comparison.

Over time, H α emission of a star forming region dissipates, and the stars can stray further away from their birth regions. Therefore, $\text{NCR}_{\text{H}\alpha}$ associations of the various CCSN subtypes have been interpreted as a tracer of the progenitor star age sequence. Type Ic SNe are thought to originate from the most massive and short-lived progenitors, which closely trace very recent star formation, and therefore the H α emission (i.e. diagonal $\text{NCR}_{\text{H}\alpha}$ distribution in Fig. 3). Other SN types present an excess in low $\text{NCR}_{\text{H}\alpha}$ values; Type IIP and IIn SNe show the strongest deviation, which indicates relatively low-mass, long-lived progenitors that no longer are associated with the H α emission of the parent stellar population. Qualitatively, the observed trend of $\text{NCR}_{\text{H}\alpha}$ statistics corresponds to the canonical understanding of the increasing progenitor mass sequence of basic CCSNe subtypes from Type IIP to Ib to Ic (e.g. [Anderson & James 2008](#); [Anderson et al. 2012](#); [Kangas et al. 2013](#)). However, as pointed out as a caveat by [Crowther \(2013\)](#), rather than probing individual H II regions, typical survey pixel scales and galaxy sample distances of NCR studies cover physical scales of a few hundred parsecs. Such scales are dominated by larger star formation complexes, which can have long, and therefore somewhat non-constraining, lifetimes of tens of millions of years. Furthermore, it is also plausible that due to projection effects massive stars with relatively low masses can be seen associated with high NCR values, or very massive stars can be hosted in isolated and faint H II regions with low NCR values. However, statistically the less massive stars with longer lifetimes are nonetheless also less likely to have high NCR values. This assumption was verified by [Kangas et al. \(2017\)](#), who found a

Table 2. Our $H\alpha$ and NUV band NCR results of the SN 1994W-like sample with the JD values of the observations and the used ON and OFF $H\alpha$ filters indicated.

SN	JD $_{H\alpha}$	ON $_{H\alpha}$	OFF $_{H\alpha}$	JD $_{NUV}$	NCR $_{H\alpha}$	NCR $_{NUV}$
1994W	2456245	#49	#52	2454241	0.182	0.554
1994ak	2456245	#49	#52	2453072	0.000	0.321
1999eb	2456244	#50	#21	2454407	0.589	0.875
1999el	2456244	#49	#52	2452875	0.000	0.440
2003G	2456244	#50	#21	2454390	0.000	0.000
2004F	2456244	#50	#21	2452972	0.624	0.647
2004gd	2456245	#50	#21	2453737	0.301	0.779
2006bo	2456244	#50	#21	2455816	0.000	0.297
2009kn	2456244	#50	#21	–	0.000	–
2011ht	2456245	#49	#52	2455304	0.000	0.478

clear correlation between NCR values of evolved massive stars and basic CCSN subtypes, consistent with the canonical picture of stellar evolution.

An intriguing NCR mapping result is that the Type II_n SN explosion sites do not follow their host galaxy $H\alpha$ emission (Anderson & James 2008; Anderson et al. 2012; Haberman et al. 2014; Ransome et al. 2022). As shown in Fig. 3, in the most extensive Type II_n NCR sample of 75 events by Ransome et al. (2022) 50% of these SNe fall in regions of 0 or very faint $H\alpha$ flux (lowest 10% bin). However, NCR values obtained by Kangas et al. (2017) for example for luminous blue variables (LBVs) in the Large Magellanic Cloud (LMC) and M 33 are higher than those of Type II_n SNe; the low NCR values imply that at least part of Type II_n SNe arise from low-mass progenitors, and the low-mass RSGs were found to have the most similar distribution to those of Type II_n SNe. However, Type II_n SNe are a heterogeneous class and a variety of progenitors is plausible (e.g. Fraser 2020).

2.2.2. NCR data

We obtained narrow-band $H\alpha$ imaging of the host galaxy sample of SN 1994W-like events using the 2.56 m Nordic Optical Telescope (NOT; Djupvik & Andersen 2010) with the Alhambra Faint Object Spectrograph and Camera (ALFOSC) equipped with a 2048×2048 pixel detector and a plate scale of $0''.19 \text{ pixel}^{-1}$ (the CCD8 detector at the time of the observations). Our sample was limited to events at a distance of <80 Mpc. Our imaging was obtained using both a narrow ‘ON’ filter that covers the $H\alpha$ line and a narrow ‘OFF’ filter close in wavelength to cover a line-free section of the continuum to subtract that from the $H\alpha$ observations. The used filters were selected based on the redshift of the host galaxy and are reported in Table 2 with the identification convention used by the NOT. The used selection of narrow-band filters included #21 ($\lambda_{\text{eff}} = 6564 \text{ \AA}$, FWHM = 33 \AA), #49 ($\lambda_{\text{eff}} = 6610 \text{ \AA}$, FWHM = 50 \AA), #50 ($\lambda_{\text{eff}} = 6653 \text{ \AA}$, FWHM = 55 \AA), and #52 ($\lambda_{\text{eff}} = 6725 \text{ \AA}$, FWHM = 60 \AA). The centre of the $H\alpha$ line is always located within the FWHM of the ON filter. The basic image reduction, including bias subtraction and flat field correction, was carried out using Image Reduction and Analysis Facility (IRAF; Tody 1986) tasks, which were also used to align the ON and OFF image pairs. The image subtraction process between the ON and OFF images of the sample galaxies was carried out with a slightly modified version of the ISIS 2.2 package (Alard & Lupton 1998; Alard 2000). This

enabled bright field stars and their surrounding background to be manually selected as reference data for the algorithm, in order to convolve the point spread function (PSF) of the higher-quality image to match that of the lower-quality image, and adjust the image levels. The world coordinate system (WCS) was derived for the analysed images using IRAF tasks and field stars listed in the USNO-A2.0 catalogue (Monet 1998), typically of the order of ~ 10 sources in the ALFOSC $6''.5 \times 6''.5$ field of view (FOV). The NCR method does not require the absolute calibration of the image, as the NCR value is defined as a fraction of emission in the galaxy from pixels fainter (or equal) to that of the target coordinates. The observed $H\alpha$ emission does include some flux from the host galaxy [N II] $\lambda\lambda 6548, 6584$ doublet; however, this effect is minimal for the NCR analysis (Kangas et al. 2017; González-Díaz et al. 2024) and applies similarly to both transient and stellar comparison samples.

2.2.3. NCR results

The resulting mean NCR $_{H\alpha}$ value of our sample of SN 1994W-like events is $\langle \text{NCR}_{H\alpha} \rangle = 0.170 \pm 0.076$, where the error is the standard error of the mean. The median distance of the sample galaxies is 60.1 Mpc, with a maximum distance of 76.8 Mpc. Our results can be compared to those of selected NCR studies with roughly similar median distances of Type IIP, Ib, and Ic SNe (at 21, 41, and 35 Mpc, respectively) by Anderson et al. (2012), and Type II_n SN samples at 38 Mpc by Haberman et al. (2014) and at 62 Mpc by Ransome et al. (2022). The main caveats in comparisons of different NCR values are related to the differences in the samples and the data. For example, if the sample distance increases, the spatial resolution decreases and the low or moderate NCR values are biased to increase while very high values may decrease. However, if the S/N ratio decreases, in particular the low NCR values are also biased to decrease. For a more detailed discussion of the caveats, see Kangas et al. (2017). The cumulative NCR $_{H\alpha}$ distribution of the sample of SN 1994W-like transients does not appear to trace the $H\alpha$ emission, and is shown in Fig. 3 in comparison to reported values from the literature for a selection of CCSN subtypes. The $\langle \text{NCR}_{H\alpha} \rangle$ value of the SN 1994W-like sample is in fact smaller than those reported for Type II_n (0.225 ± 0.058 ; 0.310 ± 0.042 , Haberman et al. 2014; Ransome et al. 2022, respectively) or Type IIP (0.264 ± 0.039 ; Anderson et al. 2012) SNe, marginally consistent within errors and subject to the distance effects. For comparison, Type Ic SNe, which are thought to arise from the massive end of the CCSN progenitor distribution, have a much stronger $H\alpha$ association (0.469 ± 0.040 ; Anderson et al. 2012) that is inconsistent with that of our sample.

As an alternative approach, we carried out the NCR analysis for the sample using the Galaxy Evolution Explorer (GALEX; Martin et al. 2005) data in the near-UV (NUV) band ($1750\text{--}2750 \text{ \AA}$) images ($1''.5 \text{ pixel}^{-1}$). The GALEX pipeline reduced data were downloaded from the GALEX data release GR6/7 archive. GALEX data were not available for ESO 561- G 020, the host galaxy of SN 2009kn. The NCR $_{NUV}$ resulted in a mean value of $\langle \text{NCR}_{NUV} \rangle = 0.488 \pm 0.084$. This is consistent with a flat distribution (mean NCR value of 0.5), similar to most CCSN subtypes with the exception of Type Ic SNe (Haberman et al. 2014, see their Figure 6). The UV light probes quite recent ($16\text{--}100$ Myr) star formation (Gogarten et al. 2009). However, this is an older star formation phase than that traced by the $H\alpha$ light, and a flat NCR $_{NUV}$ correlation for a SN subtype suggests that the bulk of their precursors have a relatively small progenitor mass. If rotating single stars in solar metallicity are

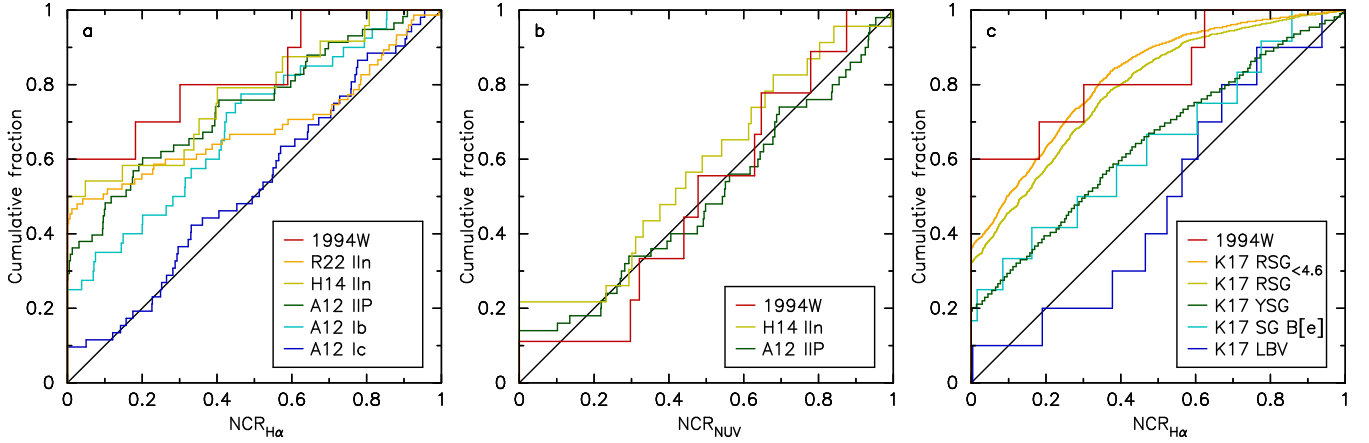


Fig. 3. NCR values of our sample of SN 1994W-like events. Comparisons include other main CCSN subtypes in a) $\text{NCR}_{\text{H}\alpha}$ and b) NCR_{NUV} (Anderson et al. 2012; Habergham et al. 2014; Ransome et al. 2022, indicated in the legend as A12, H14, and R22, respectively). In c) $\text{NCR}_{\text{H}\alpha}$ values of the SN 1994W-like sample are compared to those of a selection of massive stars in the LMC simulated at the distance of 60.1 Mpc based on the method and catalogues used by Kangas et al. (2017, indicated in the legend as K17). For RSGs, both the complete sample and a sub-sample of less massive RSGs with $\log(L/L_{\odot}) < 4.6$ are shown.

assumed, the lifetime would suggest $M_{\text{ZAMS}} \lesssim 14 M_{\odot}$ progenitors (Ekström et al. 2012). However, due to the more complex evolution of binary systems, somewhat larger masses are also possible.

We compared the $\text{NCR}_{\text{H}\alpha}$ values of SN 1994W-like events to those of a selection of different types of H-rich massive stars in the LMC. If the progenitor population of a SN type is drawn from among a particular stellar type, such stars relatively close to the end of their life cycle should have an NCR distribution consistent with that of the SNe. However, the NCR values are also influenced by factors unrelated to the stars or SNe themselves (e.g. pixel scale, spatial resolution, image depth, and SN position errors). Similar to Kangas et al. (2017), we used the $\text{H}\alpha$ image of the LMC (Gaustad et al. 2001), which we simulated to have the typical resolution and image quality of our sample host galaxy data in order to have comparable NCR distributions. This was done by i) convolving the LMC image from its original spatial resolution of 58.2 pc to that obtained by ALFOSC at the median distance of 60.1 Mpc assuming a typical seeing of $1''$ (289 pc); ii) rebinning the image from its original pixel scale of $11.6 \text{ pc pixel}^{-1}$ to that of ALFOSC at this distance with a 2×2 binning ($111 \text{ pc pixel}^{-1}$); and iii) adding noise to the image to obtain a S/N ratio similar to our ALFOSC observations in typical star-forming regions. Catalogues of different massive stars in the LMC were used, including RSGs and yellow super giants (YSGs; Neugent et al. 2012), B[e] supergiant (SG B[e]) stars (Zickgraf 2006; Bonanos et al. 2009) and LBVs (Smith & Tombleson 2015), to calculate their NCR distributions from the simulated image, adding a Gaussian positional uncertainty of $0''.5$ to their coordinates. We note the possible caveat that for example some YSGs or LBVs could be missing from the sample due to being obscured by dusty environments, which can have some effect on the NCR values. The RSGs were split into two sub-samples based on their bolometric luminosity to carry out additional comparisons.

The resulting mean $\text{NCR}_{\text{H}\alpha}$ values from the LMC data were 0.181 ± 0.012 , 0.211 ± 0.011 , 0.271 ± 0.020 , 0.355 ± 0.030 , 0.363 ± 0.089 , and 0.510 ± 0.083 for the $\text{RSG}_{\log(L/L_{\odot}) < 4.6}$ ($M_{\text{ZAMS}} \lesssim 9 M_{\odot}$ stars), RSG, $\text{RSG}_{\log(L/L_{\odot}) \geq 4.6}$, YSG, SG B[e], and LBV samples, respectively. We carried out an Anderson-Darling (AD) statistical test to compare the $\text{NCR}_{\text{H}\alpha}$ distribution of the SN 1994W-like sample to that of the selected massive star.

The resulting p values from the AD test are 27 ($\text{RSG}_{\log(L/L_{\odot}) < 4.6}$), 18 (RSG), 6 ($\text{RSG}_{\log(L/L_{\odot}) \geq 4.6}$), 7 (SG B[e]), 2 (YSG), and 1% (LBV). Therefore, the $\text{H}\alpha$ emission at the explosion sites of the SN 1994W-like sample is inconsistent with more massive stars, such as YSGs or LBVs (Fig. 3). However, the sample overlaps with the distribution of the RSGs. The NCR results also suggest that fallback explosions of relatively massive stars can be ruled out as a channel for the SN 1994W-like events.

3. Spectrophotometric evolution of SN 1999eb

3.1. SN 1999eb data

The photometric data of SN 1999eb is reported in Table A.1 and shown in Fig. 4. The observations were obtained using the 3.6 m Telescopio Nazionale Galileo (TNG) with the Optical Imager Galileo (OIG) and the ARcetri Near Infrared Camera (ARNICA), the Asiago 1.82 m Copernico Telescope with the Asiago Faint Object Spectrograph and Camera (AFOSC), the European Southern Observatory (ESO) 3.6 m telescope with the ESO Faint Object Spectrograph and Camera 2 (EFOSC2), the 8 m Very Large Telescope (VLT) with the Infrared Spectrometer And Array Camera (ISAAC; Moorwood et al. 1998a), the Danish 1.54 m telescope with the Danish Faint Object Spectrograph and Camera (DFOSC), and the 3.58 m New Technology Telescope (NTT) with the Son of ISAAC (SOFI; Moorwood et al. 1998b). Our spectroscopic log of SN 1999eb observations is reported in Table A.2 and the spectral time series is shown in Fig. 5. The data was obtained with the Asiago 1.82 m telescope with AFOSC, the ESO 3.6 m with EFOSC2, the NTT with the ESO Multi-Mode Instrument (EMMI), the 2.54 m Isaac Newton Telescope (INT) with the Intermediate Dispersion Spectrograph (IDS), and the 4.2 m William Herschel Telescope (WHT) with the Intermediate dispersion Spectrograph and Imaging System (ISIS).

Standard imaging and spectroscopic data reductions of SN 1999eb were carried out using IRAF tasks. The images were calibrated using the optical $ugri$ magnitudes of a selection of field stars from the Sloan Digital Sky Survey (SDSS; Eisenstein et al. 2011) Data Release 12 (DR12; Alam et al. 2015), and near-IR JHK magnitudes from the Two Micron All Sky Survey (2MASS; Skrutskie et al. 2006). The SDSS

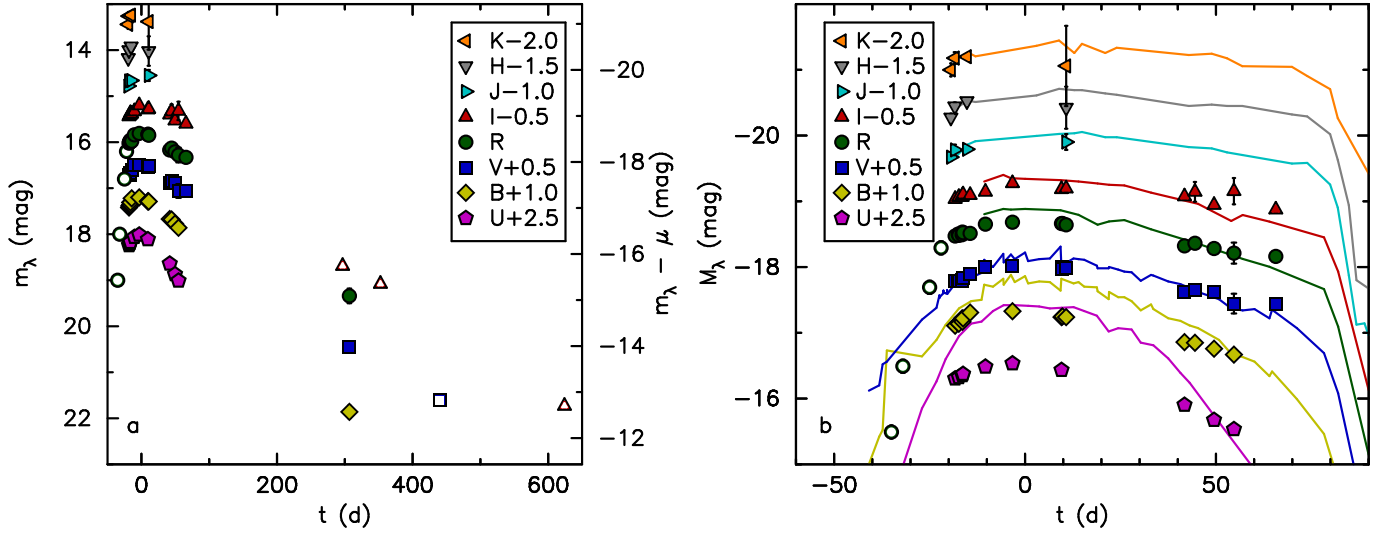


Fig. 4. a) Our observed light curves of SN 1999eb (solid symbols). For completeness, the early KAIT observations by Modjaz et al. (1999) and the late-time HST detections reported by Li et al. (2002) are also shown (open symbols). b) Absolute light curve evolution at the plateau of SN 1999eb (points) with the estimated negligible host galaxy extinction adopted. The comparison light curves (solid lines) of SN 2011ht (Roming et al. 2012; Mauerhan et al. 2013) are shown for comparison and shifted vertically by -1.6 mag.

magnitudes were converted into the Johnson-Cousins *UBVRI* system using the transformations of Jester et al. (2005). Archival *BVRI* template images of the field were made use of; images were obtained using the ESO 3.6 m telescope with EFOSC2 on 13 September 2002. The host NGC 664 is less luminous and more compact at shorter *U*-band and longer *JHK*-band wavelengths, and template subtraction was not a necessary process to carry out in these bands. The ISIS 2.2 package was used to carry out the image subtractions. The PSF photometry was carried out using a slightly modified version of the QUBA pipeline (Valenti et al. 2011). The spectra were absolute flux calibrated based on broad-band photometry, and corrected for Galactic extinction and host redshift.

3.2. SN 1999eb results

The photometry of SN 1999eb reveals a flat plateau over a time range of roughly 85 d. SN 2011ht shows a similar light curve evolution to that of SN 1999eb, although the former appears to show an intrinsic blue excess at the shortest wavelengths (Mauerhan et al. 2013). We estimated the line-of-sight host galaxy reddening of SN 1999eb with a simultaneous χ^2 fit of the *VRIJHK* light curves to those of SN 2011ht. The method has three free parameters: the host galaxy extinction, $A_{V,\text{host}}$; the intrinsic magnitude difference of the two SNe applied to all the compared bands, C ; and the time, t , at the discovery in comparison to a chosen reference point, t_0 . The 1σ errors were estimated from the χ^2 fit based probability density functions of the free parameters. For further details of the method, see Kankare et al. (2014a,b). The comparison suggests an approximate light curve maximum for SN 1999eb at JD 2451475.9, a negligible host galaxy extinction of $A_V = 0.0^{+0.2}_{-0.0}$ mag, and that SN 1999eb was $1.6^{+0.2}_{-0.1}$ mag brighter than SN 2011ht. The resulting plateau maximum for SN 1999eb is $M_R \approx -18.7$ mag. The absolute light curves of SN 1999eb at the plateau are shown in Fig. 4 with shifted light curves of SN 2011ht shown in comparison.

Non-terminal stellar outbursts are not expected to synthesize radioactive ^{56}Ni , which decays into ^{56}Co and subsequently into ^{56}Fe (e.g. Diehl & Timmes 1998), dominating

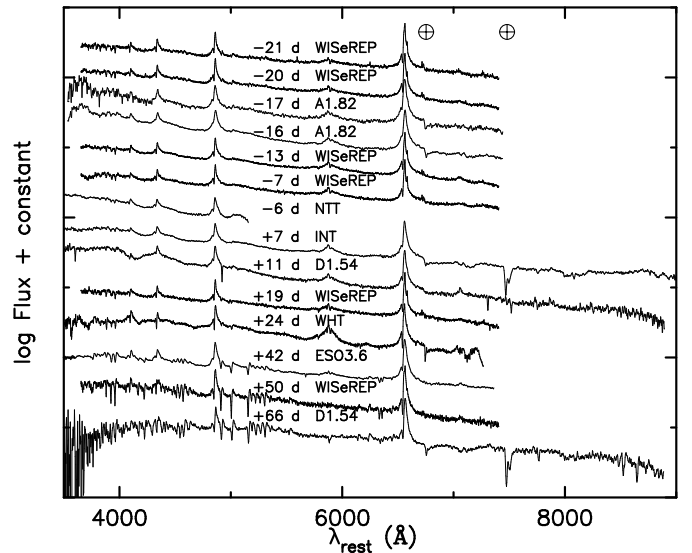


Fig. 5. Spectroscopic time series of SN 1999eb with epochs and used telescopes indicated. For completeness, the sequence includes also the public spectra on the WISeREP database (no available details on the used instruments). The spectra were dereddened by the Galactic extinction and the wavelengths corrected to the host galaxy rest frame. The wavelength of the most prominent telluric bands are indicated with a \oplus symbol. For clarity, some of the lower quality spectra were omitted from the series and the spectra have been vertically shifted.

the tail-phase light curve evolution with a theoretical bolometric luminosity decline rate of $0.98 \text{ mag } (100 \text{ d})^{-1}$ assuming complete γ -ray trapping. The late-time *I*-band decline rate of $0.94 \pm 0.01 \text{ mag } (100 \text{ d})^{-1}$ for SN 1999eb is close to this value while the *V*-band observations suggests a notably slower decline of $0.67 \pm 0.15 \text{ mag } (100 \text{ d})^{-1}$. However, SN 1999eb is also quite luminous in the late-time observations (i.e. around -13.7 , -14.5 , and -15.2 mag in *B*, *V*, and *R*-band, respectively, at $+307$ d from maximum light in the observer frame or $+302$ d in the rest frame). This suggests that some CSM interaction is likely still ongoing; unfortunately, to our knowledge,

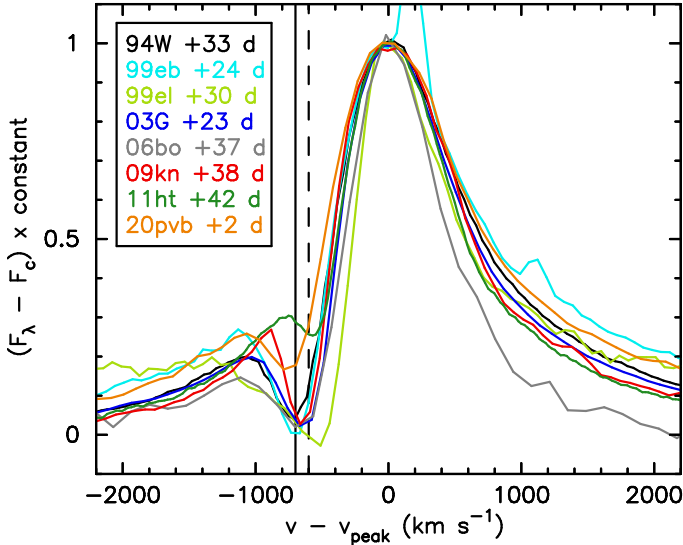


Fig. 6. Comparison of continuum-subtracted and peak-normalised $H\alpha$ profiles of SN 1994W-like events primarily around +35 d with a spectral resolution of $R \geq 800$. The $H\alpha$ lines show similarly blueshifted P Cygni absorption minima around 600–700 km s^{-1} (vertical dashed and solid lines, respectively). The spectral profile of SN 1999eb is contaminated by the host galaxy $H\alpha$ line and the effect of the feature was estimated and excluded from the normalisation process.

no spectroscopy of SN 1999eb during the tail-phase is available. We estimate a $BVRI$ pseudo-bolometric luminosity of the event using the SUPERBOL package (Nicholl 2018) at the tail phase and assume the first epoch of detection as the explosion. We find a conservative estimate for the ^{56}Ni upper limit of $<0.3 M_{\odot}$ for SN 1999eb by scaling the resulting luminosity, L_{BVRI} , to that of SN 1987A constructed from the corresponding late-time observations (Whitelock et al. 1988) and assuming a ^{56}Ni mass of $0.069 M_{\odot}$ for SN 1987A (Bouchet et al. 1991).

The typical spectral resolution of most of the observations of SN 1999eb was relatively low, within the range of $R = 200$ to 500. The spectral evolution of SN 1999eb is similar to that of SN 1994W-like events, as seen in Fig. 1. Close to light curve maximum, roughly around -20 to $+20$ d range, the spectra are dominated by strong Balmer lines with Lorentzian wings typical for electron scattering dominated emission line profiles. Furthermore, a narrow absorption component is present and has a velocity of roughly -700 km s^{-1} which is typical for SN 1994W-like events. Fig. 6 shows a compilation of $H\alpha$ line profiles of SN 1994W-like events primarily close to ~ 35 d from maximum light. The P Cygni absorption component minimum velocities are typically within ~ 600 to 700 km s^{-1} compared to the line maximum, which makes this narrow velocity range a distinct characteristic of these events. Higher-quality spectra were selected for the comparison (a spectral resolution of $R \geq 800$), since data with very low resolution will result in notable line broadening and overestimation of the velocity. For example, SNe 1994W, 2005cl, and 2011ht show a clear He I $\lambda 5875$ feature, which is also the case with SN 1999eb through the spectral sequence up to +42 d. Fe II features can be visible during the epochs covered by the spectral time series; however, spectral resolution has an effect on how prominently these lines can be detected. At the post-peak plateau phase the metal P Cygni lines become more prominent, dominated by Fe II and Ca II features, including the Ca II NIR triplet that is clearly visible in the +66 d spectrum of SN 1999eb, which is the only spectrum several tens

of days past maximum that extends sufficiently far in red wavelengths to cover this line region.

4. Early spectrophotometric nature of SN 2003G

Our observations cover two epochs of imaging of SN 2003G using the Asiago 1.82 m telescope with AFOSC. We carried out standard data reductions and PSF photometry using the QUBA pipeline. The photometry was calibrated using the $ugri$ field stars magnitudes from the SDSS DR12, converted into the $BVRI$ system (Jester et al. 2005). This resulted in the magnitudes on JD 2452664.36 of $m_B = 15.27 \pm 0.01$, $m_V = 15.15 \pm 0.04$, $m_R = 14.92 \pm 0.04$, and $m_I = 14.81 \pm 0.02$ mag, and on JD 2452696.27 of $m_B = 15.42 \pm 0.04$, $m_V = 15.26 \pm 0.03$, $m_R = 15.03 \pm 0.02$, $m_I = 14.97 \pm 0.04$ mag. The light curve reveals a rapid rise followed by a flattening, very similar to that of SN 1999eb. We carried out a simultaneous χ^2 fit of the SN 2003G $BVRI$ light curves to those of SN 1999eb, similar to the process between the latter and SN 2011ht (Sect. 3). This suggested that SN 2003G had a negligible host extinction of $A_V = 0.0^{+0.1}_{-0.0}$ mag, reached the light curve maximum around JD 2452675.7, and was 0.1 ± 0.1 mag brighter than SN 1999eb (Fig. A.1)³.

Four epochs of archival spectra of SN 2003G are available via the WISeREP database. Based on the light curve evolution of the event, the spectra have been obtained at epochs -26 , -8 , -1 , and $+23$ d from the light curve maximum, with the latter three reported by Shivers et al. (2017) in a SN sample study; these observations confirm the SN 1994W-like spectroscopic nature of the transient, as shown in Fig. 1. The -26 d spectrum of SN 2003G is distinctively redder than the spectra near maximum. A large number of P Cygni lines are visible in the -26 d spectrum with absorption minimum velocities of $\sim 500 \text{ km s}^{-1}$. Identifiable features consist of $H\alpha$, $H\beta$, Na I D, Ca II H&K, and a plethora of other metal lines, including multiplets of Fe II, Ti II, and Si II. We also suggest that the spectrum includes a few Ba II features. A P Cygni feature consistent with Ba II $\lambda 6497$ is distinctly separated from the Fe II $\lambda\lambda 6456, 6516$ lines. Ba II $\lambda 6142$ is blended with Fe II $\lambda\lambda 6148, 6149$, and Ba II $\lambda 4934$ could be blended with Fe II $\lambda 4924$. The Ba II $\lambda 4900$ line can be identified, separate from Fe II $\lambda 4924$. The Ba II lines $\lambda 4525$, $\lambda 4554$, and $\lambda 4934$ may be blended with a selection of nearby Fe II and Ti II features. Ba II $\lambda 5854$ is not prominent; however, it can be weak compared to many aforementioned Ba II features (Davidson et al. 1992). Ba II lines are commonly seen in LRNe (Blagorodnova et al. 2017, 2021; Cai et al. 2019, 2022; Pastorello et al. 2019b, 2021a,b, 2023), but also in low-luminosity Type IIP SNe (e.g. Valerin et al. 2022) and in SN 1987A-like SNe (e.g. Sit et al. 2023). Ba II lines in peculiar Type II SNe have been associated with relatively low effective temperatures (e.g. Turatto et al. 1998) and dense, low-velocity ejecta, potentially enhanced by clumping (Dessart & Hillier 2019). The -26 d spectrum of SN 2003G shows a prominent and broad absorption feature around 4300 \AA , which is seen in many SN 1994W-like events at late-plateau phases, and is likely a blend of Fe II and Ti II features (Dessart et al. 2009).

³ For completeness, we carried out a similar analysis to the two epochs of AFOSC imaging of SN 2004gd, which resulted in the magnitudes on JD 2453355.04 of $m_B = 18.64 \pm 0.07$, $m_V = 17.94 \pm 0.04$, $m_R = 17.50 \pm 0.04$, and $m_I = 17.24 \pm 0.04$ mag, and on JD 2453373.96 of $m_B = 18.96 \pm 0.05$, $m_V = 18.11 \pm 0.04$, $m_R = 17.70 \pm 0.04$, $m_I = 17.37 \pm 0.05$ mag. The light curve comparison with SN 1999eb suggested that SN 2004gd had a host extinction of $A_V = 1.0 \pm 0.2$ mag, peaked roughly around JD 2453324.5, and was $0.6^{+0.2}_{-0.1}$ mag fainter than SN 1999eb (Fig. A.1).

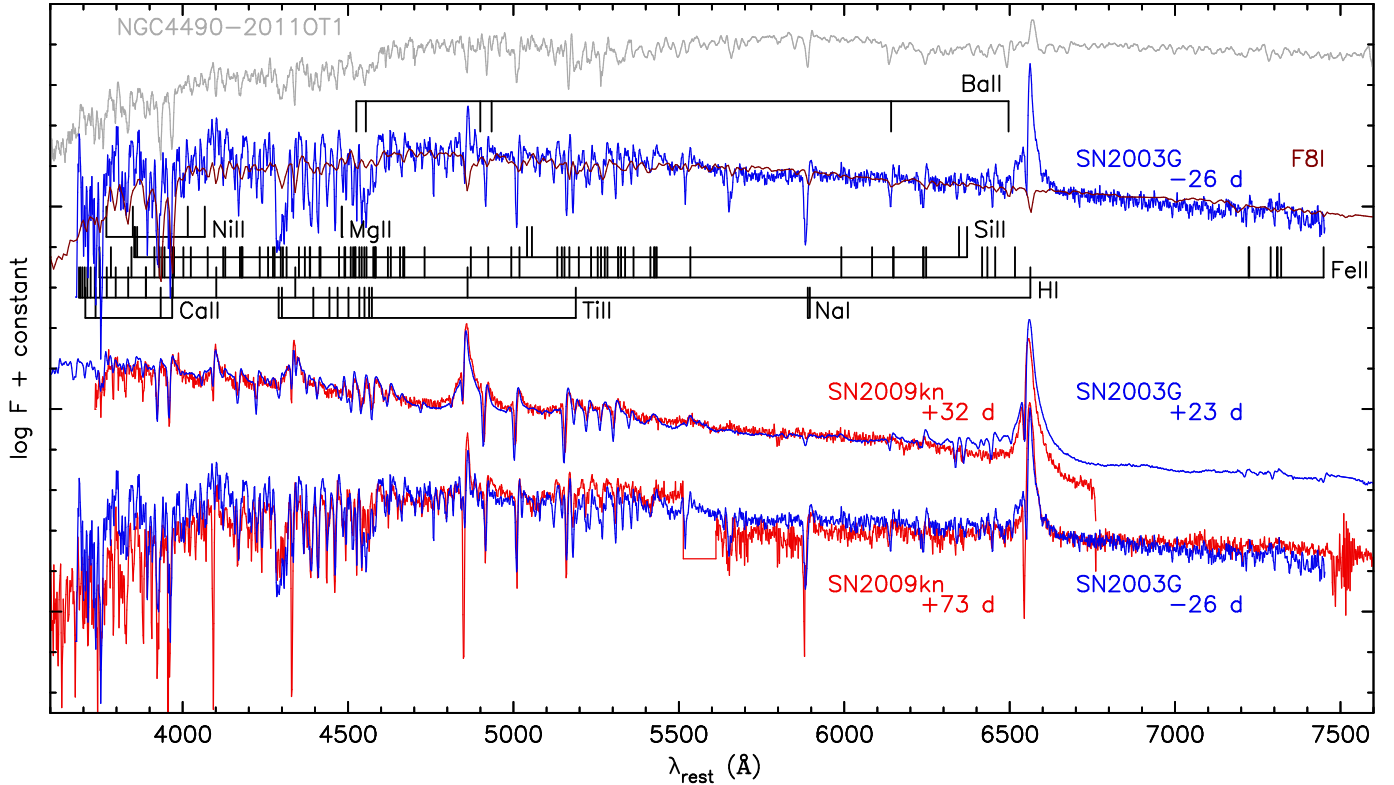


Fig. 7. Early -26 d spectrum of SN 2003G compared to LRN NGC 4490-2011OT1 close to the red maximum (Pastorello et al. 2019b), and to a F8 I type supergiant template (Pickles 1998). SN 2003G evolves spectroscopically into a SN 1994W-like event as shown by the comparison to SN 2009kn (Kankare et al. 2012). The early -26 d spectrum of SN 2003G also shows similarities to SN 1994W close to the end of the plateau at $+73$ d. A line list used by Dessart et al. (2009) to model a synthetic late-plateau spectra of SN 1994W is shown as a reference for the early spectrum of SN 2003G, in addition to our identification of the plausible Ba II features.

Pastorello et al. (2019b) noted that the very early spectrum of SN 2011ht, for which we adopted an epoch of -45 d, closely resembled the LRN NGC 4490-2011OT1 near the red, second light curve peak. Such an overall similarity is also shown by the early spectrum of SN 2003G, though the spectrum is not quite as red and in particular the $H\alpha$ line is more prominent; however, the spectrum is not obtained at as early an epoch as the first spectral observations of SN 2011ht. Nonetheless, this also shows that the early spectral characteristics of SN 2011ht are not unique among SN 1994W-like events. The -26 d spectrum of SN 2003G also shows similarities to those of SN 1994W-like events close to the end of the plateau phase, see Fig. 7. Elias-Rosa et al. (2024) reported the same effect for the similar -21 and $+31$ d spectra of SN 2020pvb. However, compared to SN 2003G, the rise time of ~ 60 d to the maximum light of SN 2020pvb is relatively long and the spectral evolution of that event is slower.

Humphreys et al. (2012) noted the similarity of the spectrum of SN 2011ht at the end of the plateau phase to those of late F-type and early G-type supergiants. Motivated by the similarity of the -26 d spectrum of SN 2003G to those of the late-plateau spectra of SN 1994W-like events, we scaled the early spectrum to the template spectra of F5 I, F8 I, G0 I, G2 I, and G5 I supergiants from Pickles (1998), and found the best match with the F8 I template; the distinctive differences are the more prominent metal line features in the SN 2003G spectrum and, in particular, the strong P Cygni Balmer lines. In Fig. 7, the spectra of SN 2003G are compared to those of LRN NGC 4490-2011OT1, type F8 I supergiant template, and SN 2009kn.

By the time of the second -8 d spectrum, SN 2003G has evolved to be bluer and the metal lines have largely disappeared,

with the exception of the most prominent Fe II lines of the $\lambda\lambda 4924, 5018, 5169$ multiplet. Furthermore, the Balmer line series has become more prominent, with less prominent absorption components compared to the overall line profiles. No major evolution is evident between the -8 and -1 d spectra (Fig. 1). The $+23$ d spectrum resembles SN 1994W-like events at early plateau, as is indicated by the strong similarity to the $+32$ d spectrum of SN 2009kn, see Fig. 7.

5. Explosion sites of SN 1994W-like transients in HST data

The Mikulski Archive for Space Telescopes was searched for high-resolution HST observations that covered the explosion site of SN 1994W-like transients. The aim was to use images to identify associated sources or set non-detection limits. The analysed data was obtained with the Wide Field and Planetary Camera 2 (WFPC2), the Advanced Camera for Surveys (ACS), or the Wide Field Camera 3 (WFC3).

5.1. Late-time HST imaging of SN 1994W

There are post-explosion HST images of the site of SN 1994W obtained with the WFPC2 in the F450W, F606W, and F814W bands on 4 July 2001, the ACS in the F814W band on 29 May 2004, and the WFC3 in the F336W band on 30 January 2011. For the first measurement of the position of SN 1994W, we used imaging of SN 1994W from the Jacobus Kapteyn Telescope (JKT) with the TEK4 instrument on 16 November 1994. The $0''.33$ pixel $^{-1}$ scale and $\sim 6' \times 6'$ FOV of the JKT image are much

larger than those of the HST data; therefore, an intermediate transformation was used to a deep *R*-band image of NGC 4401 from the NOT with ALFOSC on 14 January 2009 (kindly provided by J. Knapen), before transforming the event location to the drizzled WFPC2 F606W band mosaic. To measure the transient position in the JKT image, the local background was first fitted and subtracted with a two-dimensional polynomial. The pixel coordinates of the location were measured using three different centring algorithms in the DIGIPHOT package in IRAF, taking the average value as the event position and the standard deviation of the three values (78 mas) as the uncertainty. To identify the position of SN 1994W in the HST images, we used sources common to the JKT and the NOT, and the NOT and the HST images to derive a geometric transformation with the GEOMAP task in IRAF, allowing for shifts, rotation, and a scale factor. 14 sources common to the JKT and the NOT images were used, giving an uncertainty of $0''.26$ for the transformation; 23 sources were identified in both the NOT and WFPC2 images, giving a $0''.10$ error. The total uncertainty for the position of SN 1994W in the WFPC2 F606W band image is hence $0''.29$.

The second measurement of the position of SN 1994W was obtained from a late time image from the NOT with STAN-CAM1 on 27 January 1995. At this late epoch, the event was quite faint, and the uncertainty in its location is much larger. However, we were able to align the NOT image directly to the HST data, thus eliminating the need for an intermediate transformation. To measure the position of the SN in the NOT image, the ALFOSC *R*-band image was convolved and scaled to match the seeing of the STAN-CAM1 image, and subtracted from the latter. The centroid of SN 1994W was measured in the subtracted frame using three different algorithms as before, and transformed to the HST frame. The standard deviation of the three measurements of the position was 58 mas, while the error in the transformation was $0''.25$. Hence, the total uncertainty for the location of SN 1994W is $0''.26$.

In both cases, the position in the WFPC2 data is consistent with a relatively bright ~ 22 mag point-like source in the field (Fig. 8). DOLPHOT was used to fit a PSF to this source and the measured magnitudes are listed in Table A.3. To determine the position of SN 1994W in the ACS and WFC3 images, a transformation was determined between these images and the drizzled WFPC2 F606W mosaic. The uncertainty in this transformation was ~ 10 to 20 mas, and consequently negligible compared to the uncertainty due to the ground-based data. The superior resolution of the ACS and WFC3 data shows that the source seen in WFPC2 is comprised of a point-like source and some resolved, extended emission (Fig. 8). DOLPHOT finds a best fit to the emission complex in the ACS data using three point sources. Interestingly, the combination of the three F814W band magnitudes (24.02 ± 0.12 , 24.73 ± 0.21 , and 25.18 ± 0.32 mag) measured in the ACS image results in total $m_{F814W} = 23.34 \pm 0.11$ mag, which is consistent with the photometry of the WFPC2 image, and suggest that the source is likely a cluster or some other complex structure. The absolute magnitude of $M_{F814W} = -8.6$ mag is also consistent with what one expects for a cluster. In the WFC3 F336W band image, DOLPHOT fits the point source to the southwest with a PSF, but also fits the extended emission with 11 fainter point sources. Examination of the residual image after PSF subtraction reveals that the combination of these faint sources cleanly model the diffuse flux. The combined magnitudes of these faint sources are reported in Table A.3.

To further explore the nature of the possible cluster close to SN 1994W, we used the colour-magnitude diagram (CMD) interface to the PARSEC stellar evolutionary models (Bressan et al.

2012). The expected magnitudes in the HST filters were calculated for a cluster at solar metallicity that formed during a single burst of star formation, and the spectral energy distributions (SEDs) were scaled to match the F606W band magnitude (Fig. A.2). For population ages between 6.0 and 6.6 dex, and scaling the cluster mass to a value between 10 000 and $4300 M_{\odot}$ (where a larger scaling is needed for a younger cluster), we can match the broad-band photometry with the exception of the F336W band, which is over-predicted by the model by 1.0–1.5 mag. We disfavour an older population ($\log(\text{Age}/\text{yr}) > 6.8$ dex) as these models have redder colours at optical wavelengths. Compared to the model SEDs, the narrow-band F658N flux excess arise likely from the $H\alpha$ line emission.

The *Gaia* space observatory Data Release 3 (DR3; Gaia Collaboration 2023) report over 40 sources in the FOV of the WFC3 F336W image of the field of SN 1994W. Based on these sources, the WCS of the calibrated HST archival frame appears to be quite robust, and based on our derived pixel coordinates of the location of the transient our best estimate for the revised coordinates of SN 1994W are $\alpha = 12^{\text{h}}02^{\text{m}}11^{\text{s}}.01$ and $\delta = +62^{\circ}08'31''.8$, which we adopted for our NCR analysis (Sect. 2.2).

5.2. Late-time HST imaging of SN 1999el

SN 1999el appears as a point source in the first two epochs of HST imaging at +1.0 and +4.0 yr (Fig. 9). The field was revisited by HST at +16.1 yr and a striking light echo had developed. The echo appears broadly circular, with slightly more emission to the southwest. The diameter of the echo remains fairly constant at $\sim 0''.4$ over the seven years from +16.1 to +23.3 yr. There is no sign of the light echo in the WFC3 broad-band F110W and narrow-band F128N observations taken on 5 March 2016. Using the standard formulae to describe the radius evolution of a light echo (e.g. van Loon et al. 2004), we find that what we observe is broadly consistent with scattering by either a thin sheet or shell of dust at a radial distance of between 50 and 100 pc from SN 1999el. While SN 1999el is among the closest events in our sample, it is not possible to constrain further the properties and geometry of the scattering material; unlike in some other examples (e.g. Stritzinger et al. 2022) multiple echoes are not resolved. However, the light echo is qualitatively consistent with the high host extinction inferred towards this event. The light echo is an extended source; therefore, photometry with DOLPHOT is not feasible. However, we measured with DOLPHOT magnitudes of a selection of isolated, nearby point-like sources within a similar magnitude range to that of the light echo. We proceeded to measure these sequence sources and the light echo with aperture photometry using the Graphical Astronomy and Image Analysis (GAIA) tool with an aperture diameter of $\sim 0''.6$. Resulting magnitudes from this are reported in Table A.3. Recently, Baer-Way et al. (2024) reported HST observations of a sample of SNe and noted that SN 1999el was not detected in the F555W and F814W band observations of SN 2020dpw in NGC 6951 on 13 December 2020; it is not clear why the light echo of SN 1999el was not identified, though it could be related to the extended nature of the source.

5.3. Late-time HST imaging of SN 2011ht

Based on ground-based pre-explosion non-detections of a SN 2011ht precursor with the deepest limit of $m_g > 22.8$ mag, Roming et al. (2011) excluded LBVs in hot state, and very massive $\gtrsim 30 M_{\odot}$ YSGs and RSGs as the progenitor. We analysed

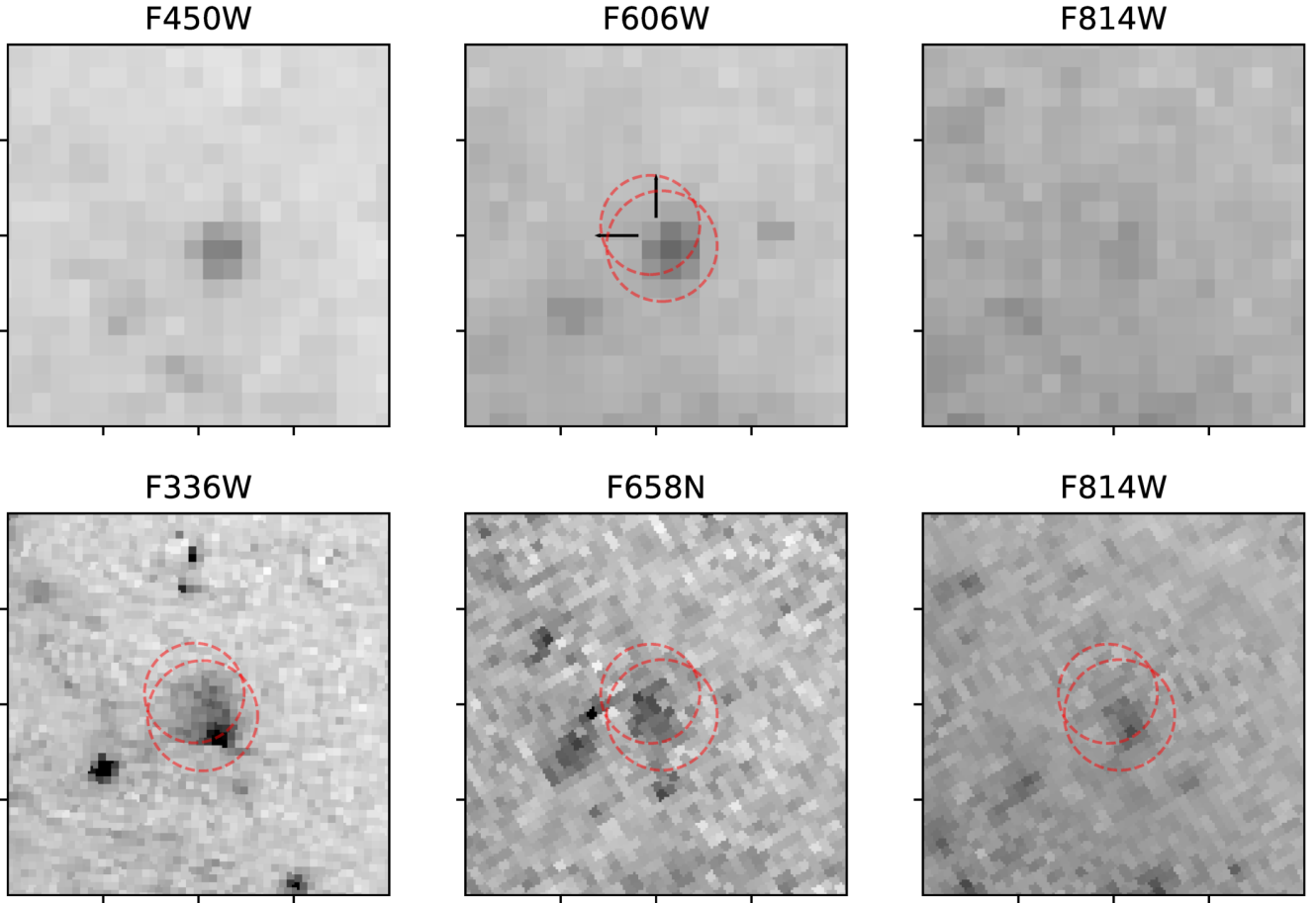


Fig. 8. 2×2 arcsec² cut-outs of the position of SN 1994W with north up and east left. The top row shows WFC2 images and the bottom row ACS and WFC3 images. The candidate host cluster of SN 1994W is most clearly seen in the F336W band, with the point-like source to the southwest, and the extended diffuse emission to the north-east. In all panels the two dashed red circles indicated the 1σ uncertainty on the transformed position of SN 1994W, as determined from the JKT and NOT images.

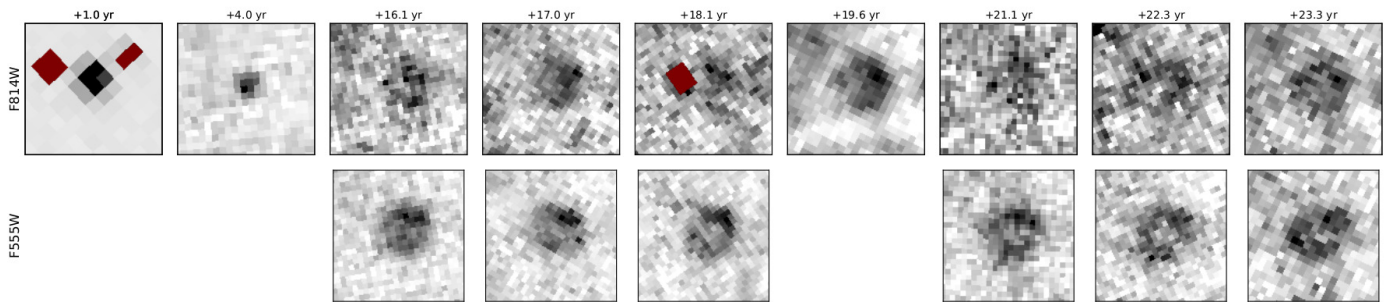


Fig. 9. Panels show 1×1 arcsec² cut-outs in the F555W and F814W bands, centred on the location of SN 1999el with north to the left and east down. Cosmic rays are masked in maroon, the phase of each image with respect to the discovery epoch is indicated above each column.

two epochs of late-time HST imaging observed with WFC3, which cover the explosion site of SN 2011ht in 10 March 2017 and 17 April 2019. No high resolution imaging is available of SN 2011ht, and hence an intermediate step was used to confirm the location of the event in these data. We downloaded the *i*-band image covering SN 2011ht taken on 13 February 2012, observed with the Panoramic Survey Telescope and Rapid Response System 1 (Pan-STARRS1; Chambers et al. 2016) telescope (PS1) using the Gigapixel Camera 1, available via the PS1 Data Release 2 (DR2) archive. This image had the best seeing available in the archive among the images where SN 2011ht was still bright. 38 sources from the *Gaia* DR3 that were located

within $10'$ of SN 2011ht were identified, and their pixel coordinates were measured on the PS1 image. Using these pixel coordinates and their corresponding *Gaia* catalogue positions, we derived a new WCS for the PS1 image. The rms uncertainty in the WCS was $0''.05$ in both α and δ . Finally, we measured the coordinates of SN 2011ht in the PS1 image, and found it to be $\alpha = 10^{\text{h}}08^{\text{m}}10^{\text{s}}.59$ and $\delta = +51^{\circ}50'57''.1$, which agrees well with those reported in the TNS.

A broadly similar process was performed for the HST images. We used the pipeline-drizzled F555W band image from 2019 as our reference. Only six *Gaia* sources fall within the FOV, and in order to account for the higher resolution compared to the

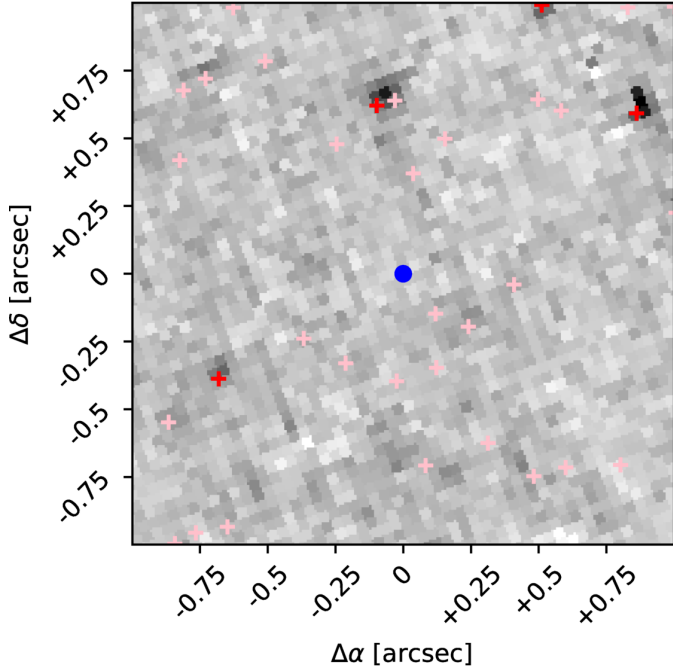


Fig. 10. 2×2 arcsec² cut-out of the drizzled F555W image with north up and east left from 10 March 2017, centred on the position of SN 2011ht (indicated with a blue circle). Sources detected at $S/N > 3$ in this image are plotted in pink, while those detected with $S/N > 5$ are plotted in red. A deep limit of $M_{F555W} > -4.0$ mag is derived for the location of the event.

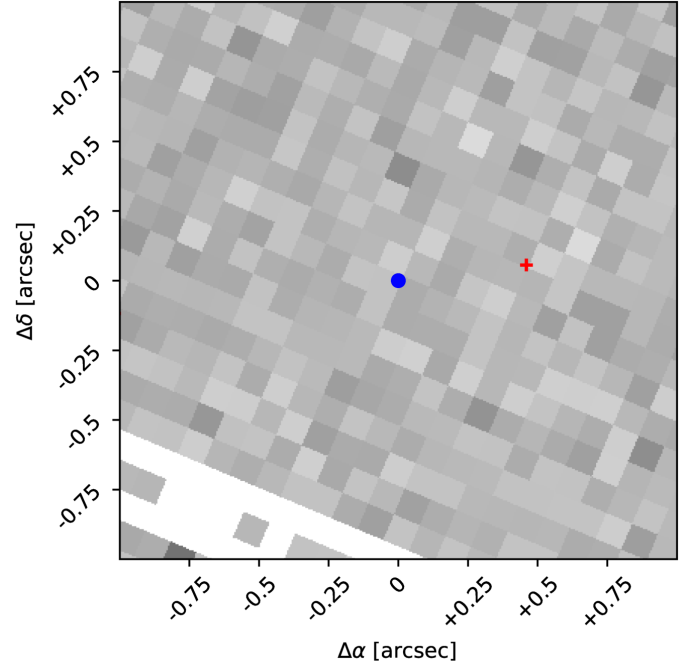


Fig. 11. 2×2 arcsec² cut-out centred on the position of SN 1994ak in the F555W band marked with a blue circle. There are no detections by DOLPHOT at $S/N > 3$; the marked source in red is associated with an imperfectly masked cosmic ray.

PS1 data, we corrected the catalogue positions for proper motion effects (the reference epoch of the *Gaia* catalogue is 2016.0, while the WFC3 image was taken 3.3 yr later). The rms error in the new WCS found for the WFC3 image is < 10 mas; therefore, the positional uncertainty is dominated by the position of SN 2011ht on the PS1 image. The new *Gaia*-derived WCS solution was used to determine the position of SN 2011ht on the WFC3 images (see Fig. 10). No source was detected within 3σ of this position. The DOLPHOT package was used to verify this, and set quantitative limits, which are reported in Table A.3. The limiting magnitude is taken from the turn over of a histogram of the number of source detected with a $S/N > 3$ as a function of magnitude, which indicates the loss of completeness. One source within 5σ of the position of SN 2011ht is marginally detected in F435W at 28.0 ± 0.3 mag. This is quite far from the position of the SN 2011ht (~ 4.3 pixels) and close to the limiting magnitude for this image at > 28.1 mag; therefore, we do not regard it as a strong associated candidate. The most constraining absolute magnitude limits for SN 2011ht are set from the 2017 images to $M_{F438W} > -3.8$ and $M_{F555W} > -4.0$ mag in the HST Vega-mag system. A luminous and very massive surviving progenitor could be expected in the scenario of interacting consecutive non-terminal outburst shells to explain SN 1994W-like events (Dessart et al. 2009); however, such a star is not identified, at least in optical wavelengths. Unless it was obscured by newly formed dust, the limits suggest that typical supergiants should be excluded as a massive surviving precursor for SN 2011ht with non-terminal outbursts.

5.4. Late-time HST imaging of SN 1994ak

The explosion site of SN 1994ak was observed with WFPC2 in the F555W and F814W bands on 18 April 1997. The WCS in

the images was verified using a single *Gaia* source that fell on the detector. DOLPHOT was run on the images, but no source was detected within $1''$ of the transient location, see Fig. 11. Similar analysis was performed on the WFC3 F225W band image obtained on 25 September 2021, and limiting magnitudes were derived similarly to those of SN 2011ht. Due to the larger distance and the less deep images, the photometry is not as constraining as that of SN 2011ht; however, the most stringent upper limits that were set are $M_{F225W} > -7.9$ and $M_{F555W} > -7.8$ mag.

5.5. Late-time HST imaging of SN 2004gd

WFC3 imaging was taken in the F225W band of the site of SN 2004gd on 10 February 2013. Due to the paucity of UV bright sources in the field, it was not possible to align these directly to an image taken of SN 2004gd. However, we verified that the WCS in the header of the HST images was correct to one or two pixels, using four *Gaia* sources in the field. Source detection was performed on the stacked, pipeline drizzled `_drc` image using DOLPHOT, while PSF-fitting photometry of each detected source was done on the individual `_flc` frames. DOLPHOT detects a number of sources in the range of $25.4 > m_{F225W} > 24.8$ mag about $0''.7$ to the west of where SN 2004gd exploded. As is seen in Fig. 12, it is likely that these are not genuine point sources, but rather marginally resolved extended emission from a bright star-forming region. At this distance of SN 2004gd, a $0''.7$ projected separation corresponds to a physical distance of at least 250 pc. No source is seen at the position of SN 2004gd itself (nor detected by DOLPHOT), and we take $m_{F225W} > 25.5$ mag (from the distribution of sources detected as a function of magnitude) as our $S/N > 3$ upper limit, corresponding to $M_{F225W} > -9.5$ mag.

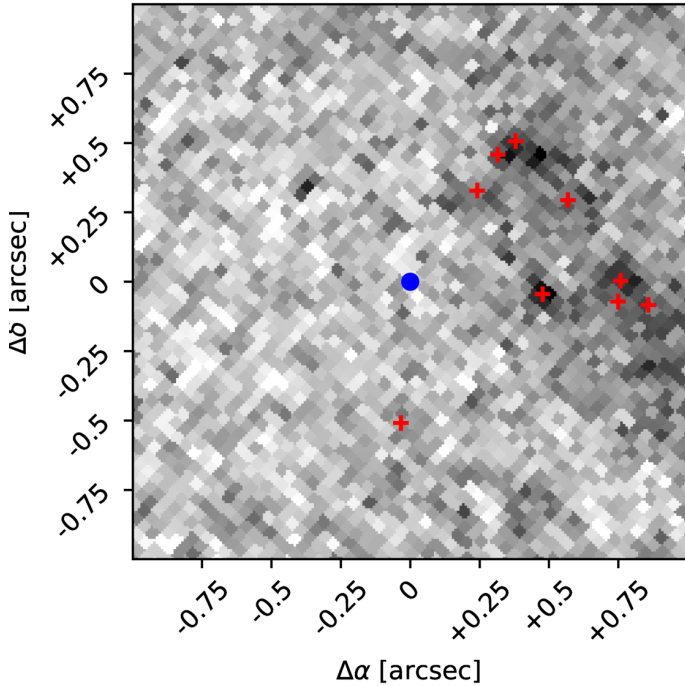


Fig. 12. 2×2 arcsec² cut-out centred on the position of SN 2004gd in the F225W band, marked with a blue circle. Sources detected by DOLPHOT at $S/N > 3$ are marked with red crosses.

6. Discussion

By expanding the sample of SN 1994W-like transients with observations of SNe 1999eb and 2003G, it was further emphasised that these events show as common characteristic narrow spectral lines with P Cygni minimum velocities of roughly $600\text{--}700\text{ km s}^{-1}$. We also identify SN 1999el as a SN 1994W-like event based on their spectroscopic similarity. Most of the sample events show a Type IIP SN-like light curve plateau followed by a sharp and deep drop, whereas SN 1999el has a more rapid Type IIL SN-like evolution, which could be related to the geometry of the CSM. The narrow spectral profiles of SN 1994W-like events are accompanied by broad emission wings, likely arising from electron scattering (Dessart et al. 2009). In the tail phase, the P Cygni absorption components and the line wings disappear. However, no broad lines are seen in the spectroscopic observations of SNe 1994W, 2009kn, and 2011ht, which extend out to the tail phase close to 200 d after maximum light (Chugai et al. 2004; Kankare et al. 2012; Mauerhan et al. 2013). Dessart et al. (2016) carried out radiation hydrodynamical modelling of a selection of different configurations of interacting transients and concluded that the interaction of a more energetic but less massive inner ejecta with a more massive CSM shell could explain the observed evolution of SN 1994W. In the $M_{\text{CSM}} > M_{\text{ejecta}}$ scenario, the inner ejecta is decelerated by the reverse shock of the interaction, converting kinetic energy efficiently into radiation, reprocessed by the slowly expanding CSM shell. At the end of the plateau phase, when the system effectively becomes optically thin, followed by a sharp light curve drop, the ejecta has already been decelerated to the bulk velocity of the CSM and no broad emission lines are seen in the tail phase spectra (see Dessart et al. 2016; Dessart 2024).

The previously reported historical outburst detections of SN 1994W-like events include the observed precursor variability before the main event of SN 2011ht (Fraser et al. 2013; Ofek et al. 2014), and one $M_w \approx -13.8$ mag PS1 detection

of SN 2020pvb roughly 111 d before the event maximum (Elias-Rosa et al. 2024). In Type II SNe, observed photons arise from different layers due to electron scattering in the ejecta. The photospheric radius, R_{phot} , defined to have a total inwardly integrated optical depth of $\tau = 2/3$, and the blackbody radius, R_{BB} , fitted to the optical observations typically deviate ($R_{\text{BB}} < R_{\text{phot}}$); Eastman et al. (1996) and Dessart & Hillier (2005) have derived temperature-dependent correction factors for this effect for normal Type IIP SNe in the context of the expanding photosphere method for distance determination. However, the corrections depend on the SN characteristics, and SN 1994W-like events are not normal Type IIP SNe. Dessart et al. (2009) carried out detailed modelling of the observed spectra of SN 1994W and reported the R_{phot} values of their synthetic spectra. We derived the R_{BB} values for the observed spectra of SN 1994W, assuming the same parameters (e.g. distance, extinction) as adopted in Dessart et al. (2009), with a blackbody fit to the spectral continuum, excluding the blue end of the spectrum ($<4670\text{ \AA}$) and wavelength regions with prominent line features. A polynomial fit to the resulting ratios of the radii yielded $R_{\text{BB}}/R_{\text{phot}} = 0.94 - 1.45(10^4/T_{\text{BB}}) + 0.87(10^4/T_{\text{BB}})^2$. The correction error was assumed to be of the order of 0.1. We carried out a similar blackbody fit to the spectra of SNe 2011ht and 2020pvb to yield the R_{BB} values and used this generic correction to roughly estimate the R_{phot} values. These radii were compared to those expected for the material ejected in the pre-outbursts of these events. When compared to the first epoch of pre-outburst detection of SN 2011ht at -367 d, and assuming the characteristic velocity of 550 km s^{-1} of the event (Fig. 6), the kinematic age of the outburst is consistent with reaching radii within which the R_{phot} can be located (Fig. 13). The expansion of the SN 2020pvb pre-outburst assuming 800 km s^{-1} is consistent within errors with the R_{BB} , though underestimated compared to the R_{phot} values; if connected, either the photosphere size is overestimated, or the pre-outburst onset happened a few hundred days earlier. The deep limits before the pre-outburst detection reported by Elias-Rosa et al. (2024) would exclude the latter scenario, unless the pre-outburst had a prominently multi-peaked light curve.

Dessart et al. (2016) discussed the possibility that a massive CSM shell of SN 1994W could have been produced by a nuclear flash that ejects the H envelope of a star in a RSG phase. Based on their modelling, Woosley & Heger (2015) suggested that in the $9.0\text{--}10.3 M_{\odot}$ range the nuclear flash from the silicon burning ignition could eject the loosely bound H envelope with velocities ranging from $\sim 10^2$ to $\sim 10^3\text{ km s}^{-1}$, with luminosities ranging from roughly $10^{39}\text{--}10^{41}\text{ erg s}^{-1}$, with delay times a couple of weeks to a couple of years to the CCSN explosion, and a likely ^{56}Ni production of $0.01\text{--}0.04 M_{\odot}$. The parameter ranges are consistent with those of the SN 2011ht pre-outburst, and the generally low ^{56}Ni mass estimates of SN 1994W-like events. Furthermore, Dessart et al. (2010) suggested based on numerical simulations that nuclear flashes could result in faint transients with a plateau-like light curve; the overall light curve evolution of the SN 2011ht pre-outburst could also be interpreted as an initial peak followed by a plateau with a red colour. The observed radiated energy of the pre-outburst of SN 2011ht was $\sim 10^{46}\text{ erg}$ based on the optical detections; however, to eject the H envelope the total energy of the outburst could have been notably larger due to the low efficiency of converting energy into radiation, and potentially considerable emission released in the longer IR wavelengths not probed by the optical observations. However, if H envelope ejecting nuclear flashes could be produced by stars in a certain mass range, it is perhaps unclear why the

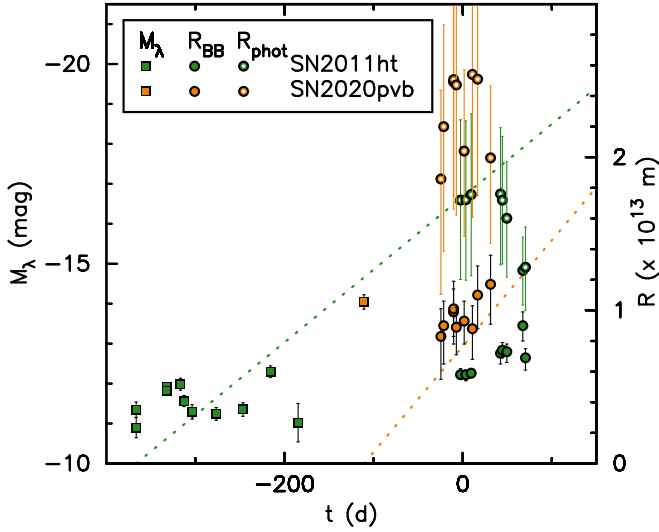


Fig. 13. Evolution of the ejecta radius assuming a 550 km s^{-1} bulk expansion velocity for a pre-outburst of SN 2011ht (dotted green line) from the onset at the first epoch of detections (square green symbols; Fraser et al. 2013; Ofek et al. 2014) compared to the estimated R_{BB} and R_{phot} evolution of the event (round closed and open green symbols, respectively) based on spectra of the event (Humphreys et al. 2012). Similarly for SN 2020pvb (in orange) based on the data by Elias-Rosa et al. (2024) assuming a velocity of 800 km s^{-1} .

SN 1994W-like events would not be more common and are quite rare instead.

Alternatively, if SN 1994W-like transients are preceded by a contact-binary-powered LRN event, this could naturally create a massive shell of CSM via ejection of the common envelope. As an example, Ercolino et al. (2024) carried out computations of binary evolution models with a $12.6 M_{\odot}$ primary, which suggested that systems with a mass ratio range of $M_2/M_1 \approx 0.25$ to 0.5 and an initial period of around 2000 d could lead to a common envelope ejection event; they also note that if such an event were to happen shortly before the SN explosion, the result could be a SN 1994W-like event. Nevertheless, to have an LRN to be followed within the timescale of roughly a year by a SN explosion would likely require a major fine-tuning of the system parameters. Therefore, with an emerging sample of several SN 1994W-like transients, generalising this scenario to all these events might be problematic, though some of the issues might be alleviated if the merging system consists of a massive star and a compact object (a neutron star or a black hole) where the latter could potentially spiral to the core relatively quickly and produce a coalescence-powered explosion (see e.g. Barkov & Komissarov 2011; Schröder et al. 2020; Brennan et al. 2025).

Regardless of the uncertainties related to the proposed models of major mass-loss episodes, our NCR results for the sample of SN 1994W-like events are most consistent with relatively low-luminosity RSG progenitors, and nuclear flash and stellar merger-powered events for the pre-outburst are consistent with a low-mass RSG origin. Based on the TNS database, the host galaxies of our sample of SN 1994W-like events have hosted also 4 Type Ia SNe, 8 unclassified transients, and 10 other CCSNe (6 Type II, 1 Type IIb, 2 Type Ib, and 1 Type Ibn SNe). Within the confirmed CCSNe, the relative distribution of subtypes is fairly similar to that of local volume-limited relative rates of CCSNe (Shivvers et al. 2017). There are some possible trends that galaxies with multiple CCSNe favour similar subtypes due

to specific star formation ages (Anderson & Soto 2013), though this appears to be a more prominent effect in highly star-forming galaxies (Kankare et al. 2021). Furthermore, our sample suffers from small number statistics; nonetheless, these galaxies have not hosted Type Ic or other Type IIIn SNe. If the hosts of SN 1994W-like transients will continue to disfavour Type Ic SNe, which are generally expected to have very massive progenitors, this would also corroborate relatively low-mass progenitors for SN 1994W-like events.

7. Conclusions

We have investigated the properties of a compilation of spectroscopically SN 1994W-like events. Our NCR sample result of $\langle \text{NCR}_{\text{H}\alpha} \rangle = 0.170 \pm 0.076$ for these transients is lower than a flat distribution that would follow the $\text{H}\alpha$ emission, which is a tracer of very recent star formation. This suggests that the progenitors of these events have longer lifetimes than the ones that trace the $\text{H}\alpha$ emission, and are therefore not very massive stars of several tens of solar masses. Instead, the NCR distribution of the sample is consistent with that of RSGs, and in particular with low-luminosity RSGs. Contrary to $\text{H}\alpha$, the SN 1994W-like transients with $\langle \text{NCR}_{\text{NUV}} \rangle = 0.488 \pm 0.084$ in our sample are consistent with a flat distribution in comparison to the host galaxy NUV emission, which is thought to trace star formation within $16\text{--}100 \text{ Myr}$, which would suggest $M_{\text{ZAMS}} \lesssim 14 M_{\odot}$ progenitors for the bulk of the SN 1994W-like events if rotating single stars in solar metallicity are assumed. However, with binary systems the possibilities are more complex, and somewhat larger masses cannot be excluded based on the NCR_{NUV} result.

We expanded the data sets of SN 1994W-like events with the analysis of SNe 1999eb and 2003G. In particular, the -26 d spectrum of SN 2003G shares similarities to spectra of F8-type supergiant stars and also to an example LRN, NGC 4490-2011OT1; furthermore, these observations show that the early spectroscopic characteristics reported for SN 2011ht are not unique among SN 1994W-like events. The early phase spectrum of SN 2003G is also remarkably similar to the spectra of SN 1994W-like events close to the end of the plateau phase, and the spectroscopic similarity between these phases of evolution appears to be a common characteristic within SN 1994W-like events.

The late-time HST data reveals the explosion sites of SNe 1994W and 1999el to be consistent with a blended $M_{\text{F814W}} = -8.6 \text{ mag}$ cluster and a ring-like ~ 0.4 diameter light echo, respectively. However, the late-time HST imaging of SN 2011ht reveals no coincident source and yields the most stringent limits for a surviving progenitor star of a SN 1994W-like event at $M_{\text{F438W}} > -3.8$ and $M_{\text{F555W}} > -4.0 \text{ mag}$, which suggests that supergiant stars should be excluded as non-terminal precursors if no major new dust formation took place that would have obscured a massive surviving star. Less constraining limits for a surviving progenitor are set for SN 1994ak and SN 2004gd at $M_{\text{F555W}} > -7.8$ and $M_{\text{F225W}} > -9.5 \text{ mag}$, respectively.

Acknowledgements. We thank the anonymous referee for useful comments. We thank Enrico Cappellaro, Luca Rizzi, Cristina Romero-Cañizales, and Marilena Salvo for the help with some of the observations. EK acknowledges financial support from the Emil Aaltonen foundation. TK acknowledges support from the Research Council of Finland project 360274. SM acknowledges support from the Research Council of Finland project 350458. AP, NER, and SB acknowledge financial support from PRIN-INAF 2022 “Shedding light on the nature of gap transients: from the observations to the models”. NER acknowledges support from the Spanish Ministerio de Ciencia e Innovación (MCIN) and the Agencia Estatal de Investigación (AEI) 10.13039/501100011033 under the program

Unidad de Excelencia María de Maeztu CEX2020-001058-M. RK acknowledges support from the Research Council of Finland project 340613. Based on observations made with the Nordic Optical Telescope, owned in collaboration by the University of Turku and Aarhus University, and operated jointly by Aarhus University, the University of Turku and the University of Oslo, representing Denmark, Finland and Norway, the University of Iceland and Stockholm University at the Observatorio del Roque de los Muchachos, La Palma, Spain, of the Instituto de Astrofísica de Canarias. The data presented here were obtained in part with ALFOSC, which is provided by the Instituto de Astrofísica de Andalucía (IAA) under a joint agreement with the University of Copenhagen and NOT. GALEX is operated for NASA by the California Institute of Technology under NASA contract NAS5-98034. Based on observations made with ESO Telescopes at the La Silla Paranal Observatory under programme IDs 67.D-0594 and 164.H-0376. Based on observations collected at Copernicus telescope (Asiago, Italy) of the INAF – Osservatorio Astronomico di Padova. Based on observations made with the WHT and INT operated on the island of La Palma by the Isaac Newton Group of Telescopes in the Spanish Observatorio del Roque de los Muchachos of the Instituto de Astrofísica de Canarias. This paper makes use of data obtained from the Isaac Newton Group of Telescopes Archive which is maintained as part of the CASU Astronomical Data Centre at the Institute of Astronomy, Cambridge. This research is based on observations made with the NASA/ESA Hubble Space Telescope obtained from the Space Telescope Science Institute, which is operated by the Association of Universities for Research in Astronomy, Inc., under NASA contract NAS 5-26555. These observations are associated with programs 6673, 8602, 9042, 9788, 12229, 13007, 14149, 14614, 14668, 15166, 15645, 16179, 16241, 16691, and 17070. The Pan-STARRS1 Surveys (PS1) and the PS1 public science archive have been made possible through contributions by the Institute for Astronomy, the University of Hawaii, the Pan-STARRS Project Office, the Max-Planck Society and its participating institutes, the Max Planck Institute for Astronomy, Heidelberg and the Max Planck Institute for Extraterrestrial Physics, Garching, The Johns Hopkins University, Durham University, the University of Edinburgh, the Queen's University Belfast, the Harvard-Smithsonian Center for Astrophysics, the Las Cumbres Observatory Global Telescope Network Incorporated, the National Central University of Taiwan, the Space Telescope Science Institute, the National Aeronautics and Space Administration under Grant No. NNX08AR22G issued through the Planetary Science Division of the NASA Science Mission Directorate, the National Science Foundation Grant No. AST-1238877, the University of Maryland, Eotvos Lorand University (ELTE), the Los Alamos National Laboratory, and the Gordon and Betty Moore Foundation. This research has made use of the NASA/IPAC Extragalactic Database (NED) which is operated by the Jet Propulsion Laboratory, California Institute of Technology, under contract with the National Aeronautics and Space Administration. This publication makes use of data products from the Two Micron All Sky Survey, which is a joint project of the University of Massachusetts and the Infrared Processing and Analysis Center/California Institute of Technology, funded by the National Aeronautics and Space Administration and the National Science Foundation. Funding for SDSS-III has been provided by the Alfred P. Sloan Foundation, the Participating Institutions, the National Science Foundation, and the U.S. Department of Energy Office of Science. The SDSS-III web site is <http://www.sdss3.org/>. SDSS-III is managed by the Astrophysical Research Consortium for the Participating Institutions of the SDSS-III Collaboration including the University of Arizona, the Brazilian Participation Group, Brookhaven National Laboratory, Carnegie Mellon University, University of Florida, the French Participation Group, the German Participation Group, Harvard University, the Instituto de Astrofísica de Canarias, the Michigan State/Notre Dame/JINA Participation Group, Johns Hopkins University, Lawrence Berkeley National Laboratory, Max Planck Institute for Astrophysics, Max Planck Institute for Extraterrestrial Physics, New Mexico State University, New York University, Ohio State University, Pennsylvania State University, University of Portsmouth, Princeton University, the Spanish Participation Group, University of Tokyo, University of Utah, Vanderbilt University, University of Virginia, University of Washington, and Yale University. GAIA is a derivative of the Skycat catalogue and image display tool, developed as part of the VLT project at ESO. Skycat and GAIA are free software under the terms of the GNU copyright. We have made use of the Weizmann interactive supernova data repository (www.weizmann.ac.il/astrophysics/wiserep). We have made use of the Ned Wright's cosmology calculator (Wright 2006, www.astro.ucla.edu/~wright/CosmoCalc.html).

References

- Alam, S., Albareti, F. D., Allende Prieto, C., et al. 2015, *ApJS*, 219, 12
- Alard, C. 2000, *A&AS*, 144, 363
- Alard, C., & Lupton, R. H. 1998, *ApJ*, 503, 325
- Anderson, J. P., & James, P. A. 2008, *MNRAS*, 390, 1527
- Anderson, J. P., & Soto, M. 2013, *A&A*, 550, A69
- Anderson, J. P., Haberman, S. M., James, P. A., & Hamuy, M. 2012, *MNRAS*, 424, 1372
- Baer-Way, R., DeGraw, A., Zheng, W., et al. 2024, *ApJ*, 964, 172
- Barkov, M. V., & Komissarov, S. S. 2011, *MNRAS*, 415, 944
- Bennett, C. L., Larson, D., Weiland, J. L., & Hinshaw, G. 2014, *ApJ*, 794, 135
- Bietenholz, M. F., Bartel, N., Argo, M., et al. 2021, *ApJ*, 908, 75
- Blagorodnova, N., Kotak, R., Polshaw, J., et al. 2017, *ApJ*, 834, 107
- Blagorodnova, N., Kléncki, J., Pejcha, O., et al. 2021, *A&A*, 653, A134
- Blondin, S., Modjaz, M., Kirshner, R., Challis, P., & Hernandez, J. 2006, *Cent. Bur. Electron. Telegrams*, 481, 1
- Boles, T., & Monard, L. A. G. 2006, *Cent. Bur. Electron. Telegrams*, 468, 1
- Boles, T., Pastorello, A., Stanishev, V., et al. 2011, *Cent. Bur. Electron. Telegrams*, 2851, 1
- Bonanos, A. Z., Massa, D. L., Sewilo, M., et al. 2009, *AJ*, 138, 1003
- Bouchet, P., Phillips, M. M., Suntzeff, N. B., et al. 1991, *A&A*, 245, 490
- Bragaglia, A., Munari, U., Barbon, R., et al. 1994, *IAU Circ.*, 6044, 1
- Brennan, S. J., Bartmentloo, S., Schulze, S., et al. 2025, *A&A*, submitted [arXiv:2503.08768]
- Bressan, A., Marigo, P., Girardi, L., et al. 2012, *MNRAS*, 427, 127
- Cai, Y.-Z., Pastorello, A., Fraser, M., et al. 2019, *A&A*, 632, L6
- Cai, Y.-Z., Pastorello, A., Fraser, M., et al. 2022, *A&A*, 667, A4
- Cao, L., Qiu, Y. L., Qiao, Q. Y., et al. 1999, *IAU Circ.*, 7288, 1
- Chambers, K. C., Magnier, E. A., Metcalfe, N., et al. 2016, ArXiv e-prints [arXiv:1612.05560]
- Chambers, K. C., Boer, T. D., Bulger, J., et al. 2020, *TNSTR*, 2201, 1
- Chugai, N. N., Blinnikov, S. I., Cumming, R. J., et al. 2004, *MNRAS*, 352, 1213
- Cortini, G., Villi, M., Barbon, R., et al. 1994, *IAU Circ.*, 6042, 1
- Crowther, P. A. 2013, *MNRAS*, 428, 1927
- Davidson, M. D., Snoek, L. C., Volten, H., & Doenselmann, A. 1992, *A&A*, 255, 457
- de Jaeger, T., Anderson, J. P., Pignata, G., et al. 2015, *ApJ*, 807, 63
- Dessart, L. 2024, ArXiv e-prints [arXiv:2405.04259]
- Dessart, L., & Hillier, D. J. 2005, *A&A*, 439, 671
- Dessart, L., & Hillier, D. J. 2019, *A&A*, 622, A70
- Dessart, L., Hillier, D. J., Gezari, S., et al. 2009, *MNRAS*, 394, 21
- Dessart, L., Livne, E., & Waldman, R. 2010, *MNRAS*, 405, 2113
- Dessart, L., Hillier, D. J., Audit, E., et al. 2016, *MNRAS*, 458, 2094
- Di Carlo, E., Massi, F., Valentini, G., et al. 2002, *ApJ*, 573, 144
- Diehl, R., & Timmes, F. X. 1998, *PASP*, 110, 637
- Djupvik, A. A., & Andersen, J. 2010, *Highlights of Spanish Astrophysics V*, 14, 211
- Dolphin, A. E. 2000, *PASP*, 112, 1383
- Drake, S. A., & Ulrich, R. K. 1980, *ApJS*, 42, 351
- Eastman, R. G., Schmidt, B. P., & Kirshner, R. 1996, *ApJ*, 466, 911
- Eisenstein, D. J., Weinberg, D. H., Agol, E., et al. 2011, *AJ*, 142, 72
- Ekström, S., Georgy, C., Eggenberger, P., et al. 2012, *A&A*, 537, A146
- Elias-Rosa, N., Brennan, S. J., Benetti, S., et al. 2024, *A&A*, 686, A13
- Ercolino, A., Jin, H., Langer, N., et al. 2024, *A&A*, 685, A58
- Fassia, A., Meikle, W. P. S., Chugai, N., et al. 2001, *MNRAS*, 325, 907
- Filippenko, A. V. 1997, *ARA&A*, 35, 309
- Filippenko, A. V., & Barth, A. J. 1994, *IAU Circ.*, 6046, 2
- Filippenko, A. V., & Foley, R. J. 2004, *IAU Circ.*, 8453, 3
- Filippenko, A. V., Chornock, R., Foley, R. J., & Li, W. 2004, *IAU Circ.*, 8288, 2
- Fraser, M. 2020, *R. Soc. Open Sci.*, 7, 200467
- Fraser, M., Magee, M., Kotak, R., et al. 2013, *ApJ*, 779, L8
- Fruchter, A. S., Levan, A. J., Strolger, L., et al. 2006, *Nature*, 441, 463
- Gagliano, R., Newton, J., Puckett, T., et al. 2009, *Cent. Bur. Electron. Telegrams*, 1997, 1
- Gaia Collaboration (Vallenari, A., et al.) 2023, *A&A*, 674, A1
- Garnavich, P., Challis, P., Riess, A., Kirshner, R., & Berlind, P. 1995, *IAU Circ.*, 6124, 3
- Garnavich, P., Jha, S., Challis, P., Kirshner, R., & Berlind, P. 1999, *IAU Circ.*, 7268, 2
- Gaustad, J. E., McCullough, P. R., Rosing, W., & Van Buren, D. 2001, *PASP*, 113, 1326
- Gogarten, S. M., Dalcanton, J. J., Williams, B. F., et al. 2009, *ApJ*, 691, 115
- González-Díaz, R., Galbany, L., Kangas, T., et al. 2024, *A&A*, 684, A104
- Graham, J., Li, W., Puckett, T., et al. 2003, *IAU Circ.*, 8045, 1
- Haberman, S. M., Anderson, J. P., James, P. A., & Lyman, J. D. 2014, *MNRAS*, 441, 2230
- Hamuy, M., & Maza, J. 2003, *IAU Circ.*, 8045, 2
- Humphreys, R. M., Davidson, K., Jones, T. J., et al. 2012, *ApJ*, 760, 93
- Ivanova, N., Justham, S., Avendano Nandez, J. L., & Lombardi, J. C. 2013, *Science*, 339, 433
- James, P. A., & Anderson, J. P. 2006, *A&A*, 453, 57
- Jester, S., Schneider, D. P., Richards, G. T., et al. 2005, *AJ*, 130, 873
- Kangas, T., Mattila, S., Kankare, E., et al. 2013, *MNRAS*, 436, 3464
- Kangas, T., Portinari, L., Mattila, S., et al. 2017, *A&A*, 597, A92

- Kankare, E., Ergon, M., Bufano, F., et al. 2012, *MNRAS*, 424, 855
- Kankare, E., Fraser, M., Ryder, S., et al. 2014a, *A&A*, 572, A75
- Kankare, E., Mattila, S., Ryder, S., et al. 2014b, *MNRAS*, 440, 1052
- Kankare, E., Efstathiou, A., Kotak, R., et al. 2021, *A&A*, 649, A134
- Kiewe, M., Gal-Yam, A., Arcavi, I., et al. 2012, *ApJ*, 744, 10
- Li, C., & Morozova, V. 2022, *MNRAS*, 515, 3597
- Li, W., Filippenko, A. V., Van Dyk, S. D., et al. 2002, *PASP*, 114, 403
- Lipunov, V. M., Blinnikov, S., Gorbovskoy, E., et al. 2017, *MNRAS*, 470, 2339
- MacLeod, M., Macias, P., Ramirez-Ruiz, E., et al. 2017, *ApJ*, 835, 282
- Martin, D. C., Fanson, J., Schiminovich, D., et al. 2005, *ApJ*, 619, L1
- Matsumoto, T., & Metzger, B. D. 2022, *ApJ*, 938, 5
- Mauerhan, J. C., Smith, N., Silverman, J. M., et al. 2013, *MNRAS*, 431, 2599
- Metzger, B. D., & Pejcha, O. 2017, *MNRAS*, 471, 3200
- Modjaz, M., Li, W. D., Garnavich, P., et al. 1999, *IAU Circ.*, 7268, 1
- Modjaz, M., Kirshner, R., Challis, P., et al. 2005, *IAU Circ.*, 8544, 4
- Monet, D. 1998, *Am. Astron. Soc. Meet. Abstr.*, 30, 1427
- Moore, M., Shimasaki, K., & Li, W. 2004, *IAU Circ.*, 8443, 3
- Moorwood, A., Cuby, J.-G., Biereichel, P., et al. 1998a, *Messenger*, 94, 7
- Moorwood, A., Cuby, J.-G., & Lidman, C. 1998b, *Messenger*, 91, 9
- Moriya, T. J., Tominaga, N., Langer, N., et al. 2014, *A&A*, 569, A57
- Mould, J. R., Huchra, J. P., Freedman, W. L., et al. 2000, *ApJ*, 529, 786
- Nakano, S., Kushida, R., & Kushida, Y. 1994, *IAU Circ.*, 6122, 3
- Neugent, K. F., Massey, P., Skiff, B., & Meynet, G. 2012, *ApJ*, 749, 177
- Nicholl, M. 2018, *Res. Notes Am. Astron. Soc.*, 2, 230
- Ofek, E. O., Sullivan, M., Shaviv, N. J., et al. 2014, *ApJ*, 789, 104
- Pastorello, A., Turatto, M., Benetti, S., et al. 2002, *MNRAS*, 333, 27
- Pastorello, A., Stanishev, V., Smartt, S. J., et al. 2011, *Cent. Bur. Electron. Telegrams*, 2851, 2
- Pastorello, A., Chen, T.-W., Cai, Y.-Z., et al. 2019a, *A&A*, 625, L8
- Pastorello, A., Mason, E., Taubenberger, S., et al. 2019b, *A&A*, 630, A75
- Pastorello, A., Fraser, M., Valerin, G., et al. 2021a, *A&A*, 646, A119
- Pastorello, A., Valerin, G., Fraser, M., et al. 2021b, *A&A*, 647, A93
- Pastorello, A., Valerin, G., Fraser, M., et al. 2023, *A&A*, 671, A158
- Perley, D. A., Taggart, K., Dahiwal, A., et al. 2020, *TNS Classif. Rep.*, 3139, 1
- Pickles, A. J. 1998, *PASP*, 110, 863
- Prieto, J. L., McMillan, R., Bakos, G., et al. 2011, *Cent. Bur. Electron. Telegrams*, 2903, 1
- Pugh, H., & Li, W. 2005, *IAU Circ.*, 8544, 3
- Ransome, C. L., Habergham-Mawson, S. M., Darnley, M. J., James, P. A., & Percival, S. M. 2022, *MNRAS*, 513, 3564
- Roming, P., Pritchard, T., & Brown, P. 2011, *ATel*, 3690, 1
- Roming, P. W. A., Pritchard, T. A., Prieto, J. L., et al. 2012, *ApJ*, 751, 92
- Schlafly, E. F., & Finkbeiner, D. P. 2011, *ApJ*, 737, 103
- Schröder, S. L., MacLeod, M., Loeb, A., et al. 2020, *ApJ*, 892, 13
- Shivvers, I., Modjaz, M., Zheng, W., et al. 2017, *PASP*, 129, 054201
- Sit, T., Kasliwal, M. M., Tzanidakis, A., et al. 2023, *ApJ*, 959, 142
- Skrutskie, M. F., Cutri, R. M., Stiening, R., et al. 2006, *AJ*, 131, 1163
- Smith, N., & Tombleson, R. 2015, *MNRAS*, 447, 598
- Smith, N., Andrews, J. E., Van Dyk, S. D., et al. 2016, *MNRAS*, 458, 950
- Sollerman, J., Cumming, R. J., & Lundqvist, P. 1998, *ApJ*, 493, 933
- Steele, T. N., Cobb, B., & Filippenko, A. V. 2009, *Cent. Bur. Electron. Telegrams*, 2011, 1
- Stritzinger, M. D., Taddia, F., Fraser, M., et al. 2020, *A&A*, 639, A104
- Stritzinger, M. D., Taddia, F., Lawrence, S. S., et al. 2022, *ApJ*, 939, L8
- Swift, B., Burket, J., Pugh, H., et al. 2004, *IAU Circ.*, 8271, 2
- Taddia, F., Stritzinger, M. D., Sollerman, J., et al. 2013, *A&A*, 555, A10
- Tody, D. 1986, *Proc. SPIE*, 627, 733
- Turatto, M., Mazzali, P. A., Young, T. R., et al. 1998, *ApJ*, 498, L129
- Tylenda, R., Hajduk, M., Kamiński, T., et al. 2011, *A&A*, 528, A114
- Valenti, S., Fraser, M., Benetti, S., et al. 2011, *MNRAS*, 416, 3138
- Valerin, G., Pumo, M. L., Pastorello, A., et al. 2022, *MNRAS*, 513, 4983
- van Loon, J. T., Evans, A., Rushton, M. T., & Smalley, B. 2004, *A&A*, 427, 193
- Whitelock, P. A., Catchpole, R. M., Menzies, J. W., et al. 1988, *MNRAS*, 234, 5
- Woosley, S. E., & Heger, A. 2015, *ApJ*, 810, 34
- Woosley, S. E., Heger, A., & Weaver, T. A. 2002, *Rev. Mod. Phys.*, 74, 1015
- Wright, E. L. 2006, *PASP*, 118, 1711
- Yaron, O., & Gal-Yam, A. 2012, *PASP*, 124, 668
- Zickgraf, F.-J. 2006, *ASP Conf. Ser.*, 355, 135

Appendix A: Additional tables and figures

Table A.1. New photometry for SN 1999eb with the errors given in brackets.

JD	m_U (mag)	m_B (mag)	m_V (mag)	m_R (mag)	m_I (mag)	m_J (mag)	m_H (mag)	m_K (mag)	Telescope
2451456.48	-	-	-	-	-	15.78(0.06)	15.67(0.06)	15.44(0.10)	TNG/ARNICA
2451457.51	-	-	-	-	-	15.67(0.08)	15.50(0.06)	15.26(0.09)	TNG/ARNICA
2451457.59	15.74(0.02)	16.42(0.02)	16.22(0.03)	16.02(0.05)	15.94(0.04)	-	-	-	TNG/OIG
2451458.39	-	16.38(0.02)	16.22(0.02)	15.99(0.03)	-	-	-	-	AS1.82/AFOSC
2451458.56	15.72(0.04)	16.39(0.02)	16.22(0.04)	16.01(0.05)	15.91(0.04)	-	-	-	TNG/OIG
2451459.41	-	16.31(0.03)	16.20(0.01)	16.00(0.03)	15.91(0.04)	-	-	-	AS1.82/AFOSC
2451459.50	15.69(0.05)	16.36(0.01)	16.22(0.02)	15.96(0.05)	15.89(0.03)	-	-	-	TNG/OIG
2451459.66	15.67(0.05)	16.31(0.03)	16.17(0.01)	15.97(0.03)	15.87(0.04)	-	-	-	ESO3.6/EFOSC2
2451460.67	-	-	-	-	-	15.66(0.04)	15.42(0.04)	15.24(0.04)	VLT/ISAAC
2451461.51	-	16.22(0.03)	16.11(0.03)	15.98(0.05)	15.88(0.05)	-	-	-	AS1.82/AFOSC
2451465.51	15.56(0.04)	-	16.00(0.03)	15.84(0.05)	15.83(0.04)	-	-	-	TNG/OIG
2451472.61	15.51(0.05)	16.20(0.02)	15.99(0.01)	15.81(0.02)	15.70(0.02)	-	-	-	D1.54/DFOSC
2451485.45	15.61(0.05)	16.29(0.01)	16.01(0.03)	15.83(0.05)	15.79(0.04)	-	-	-	TNG/OIG
2451485.70	-	16.28(0.02)	16.03(0.01)	15.83(0.02)	-	-	-	-	D1.54/DFOSC
2451486.66	-	16.29(0.02)	16.02(0.01)	15.85(0.02)	15.78(0.03)	-	-	-	D1.54/DFOSC
2451486.68	-	-	-	-	-	15.55(0.12)	15.52(0.32)	15.38(0.61)	NTT/SOFI
2451517.66	16.14(0.05)	16.67(0.02)	16.39(0.03)	16.17(0.05)	15.90(0.04)	-	-	-	ESO3.6/EFOSC2
2451520.40	-	16.68(0.03)	16.35(0.03)	16.13(0.02)	15.83(0.15)	-	-	-	AS1.82/AFOSC
2451525.40	16.37(0.05)	16.77(0.02)	16.39(0.03)	16.21(0.05)	16.03(0.04)	-	-	-	TNG/OIG
2451530.61	16.51(0.08)	16.86(0.05)	16.56(0.15)	16.28(0.16)	15.82(0.20)	-	-	-	ESO3.6/EFOSC2
2451541.57	-	-	16.57(0.01)	16.33(0.02)	16.10(0.03)	-	-	-	D1.54/DFOSC
2451782.69	-	20.86(0.14)	19.96(0.07)	19.34(0.16)	-	-	-	-	TNG/OIG

Table A.2. Spectroscopic log of observations for SN 1999eb.

JD	t (d)	Grism/grating	Slit (")	R	$t_{\text{integration}}$ (s)	Telescope
2451458.5	-17	GR04	2.1	290	1800	AS1.82/AFOSC
2451459.5	-16	GR04	2.1	290	2800+2700	AS1.82/AFOSC
2451459.7	-16	Gr#11	1.5	230	600	ESO3.6/EFOSC2
2451469.7	-6	Grat#5	1.0	400	2×600	NTT/EMMI
2451482.5	+7	R150V	1.5	330	4×1800	INT/IDS
2451485.7	+10	Gr#4	1.5	470	3600	D1.54/DFOSC
2451486.7	+11	Gr#4	1.5	470	3600	D1.54/DFOSC
2451489.7	+24	R300B, R316R	1.0	1100, 1800	1200	WHT/ISIS
2451517.6	+42	Gr#11	1.5	230	1200	ESO3.6/EFOSC2
2451541.6	+66	Gr#4	2.0	470	1800	D1.54/DFOSC

Table A.3. Late-time HST photometry of the explosion sites of SN 1994W-like events with the errors given in brackets.

SN	Date (UT)	JD	m_{F225W} (mag)	m_{F336W} (mag)	m_{F438W} (mag)	m_{F450W} (mag)	m_{F555W} (mag)	m_{F606W} (mag)	m_{F658N} (mag)	m_{F814W} (mag)	Instrument
1994W	2001-07-04.8	2452095.3	-	-	-	22.76(0.06)	-	22.99(0.05)	-	23.53(0.18)	WFPC2
1994W	2004-05-29.6	2453155.1	-	-	-	-	-	-	22.58(0.18)	23.34(0.11)	ACS
1994W	2011-01-30.0	2455591.5	-	22.43(0.11)	-	-	-	-	-	-	WFC3
1994ak	1997-04-18.4	2450556.9	-	-	-	-	>25.3	-	-	>24.3	WFPC2
1994ak	2021-09-25.1	2459482.6	>25.3	-	-	-	-	-	-	-	WFC3
1999el	2003-10-24.5	2452937.0	-	-	-	-	-	-	-	23.64(0.17)	ACS
1999el	2015-11-25.6	2457352.1	-	-	-	-	24.13(0.22)	-	-	23.89(0.23)	WFC3
1999el	2016-10-15.0	2457676.5	-	-	-	-	24.11(0.28)	-	-	23.70(0.18)	WFC3
1999el	2017-11-10.8	2458068.3	-	-	-	-	24.23(0.25)	-	-	23.75(0.25)	WFC3
1999el	2019-05-23.0	2458626.5	-	-	-	-	-	-	-	24.03(0.30)	ACS
1999el	2020-12-13.9	2459197.4	-	-	-	-	24.33(0.21)	-	-	23.95(0.27)	WFC3
1999el	2022-02-17.1	2459627.6	-	-	-	-	24.40(0.25)	-	-	23.96(0.23)	WFC3
1999el	2023-02-22.3	2459997.8	-	-	-	-	24.33(0.30)	-	-	24.07(0.29)	ACS
2004gd	2013-02-10.8	2456334.3	>25.5	-	-	-	-	-	-	-	WFC3
2011ht	2017-03-10.6	2457823.1	>26.5	-	>28.1	-	>27.9	-	-	>27.0	WFC3
2011ht	2019-04-17.1	2458590.6	-	-	-	-	>27.4	-	-	>26.3	WFC3

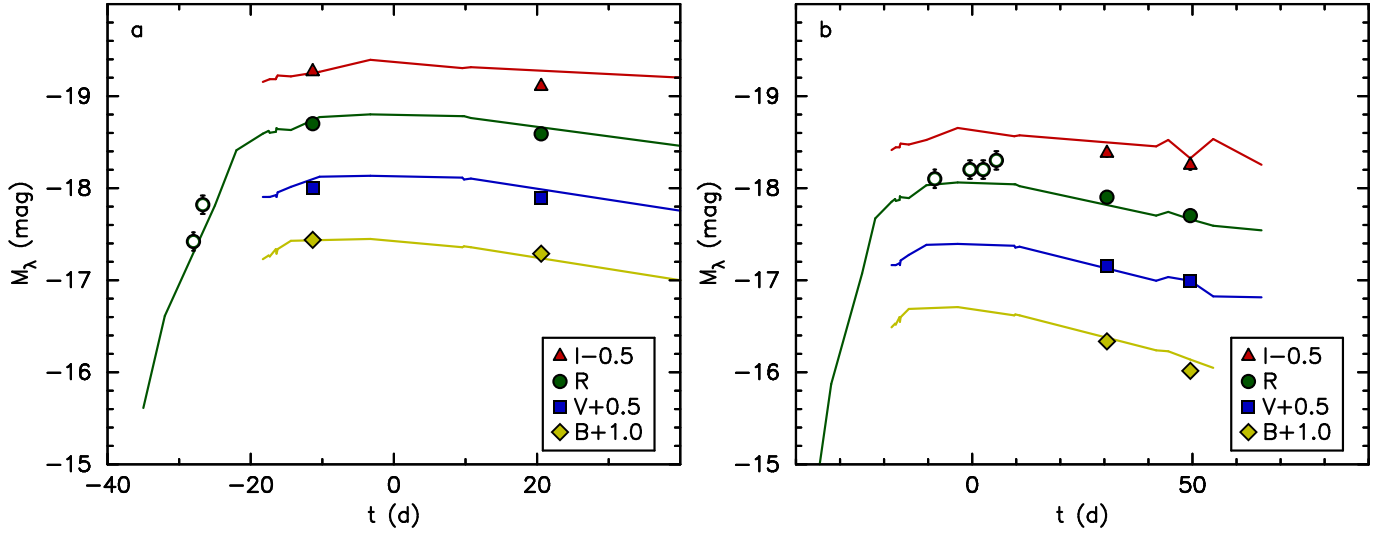


Fig. A.1. a) Absolute light curves of SN 2003G (points) with the estimated negligible host galaxy extinction adopted. The early observations by Graham et al. (2003) are shown with open symbols. The comparison light curves (solid lines) of SN 1999eb (Sect. 3) are shown vertically shifted by -0.1 mag. b) Absolute light curves of SN 2004gd (points) with the estimated host galaxy extinction of $A_V = 1.0$ mag; the photometry of the event was carried out with Pan-STARRS1 DR2 images as rough templates. The early observations by Moore et al. (2004) are shown with open symbols. The comparison light curves (solid lines) of SN 1999eb are shown vertically shifted by $+0.6$ mag.

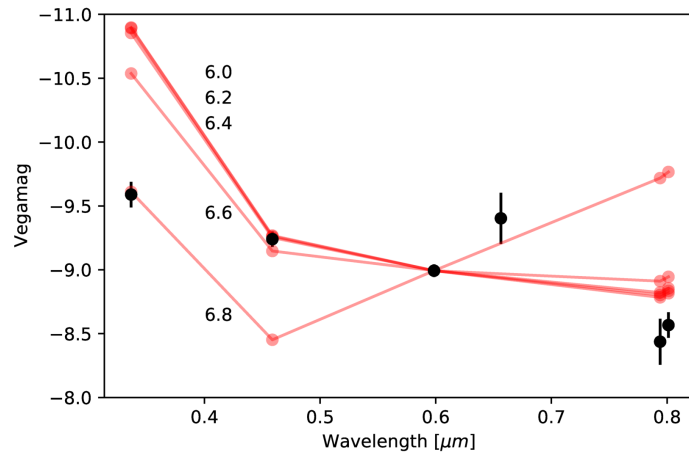


Fig. A.2. SED fits to photometry of the putative host cluster of SN 1994W. The combined magnitude of both the point source and any diffuse emission is shown at the wavelength of each band. SED models have been scaled to match the F606W band, and are plotted in red. We see that populations with $\log(\text{Age})$ between 6.0 and 6.6 dex match, with the exception of the F336W band, while the older 6.8 dex population does not match either the F450W or the F814W band.